ARTICLE

Simultaneously targeting cancer-associated fibroblasts and angiogenic vessel as a treatment for TNBC

Malvika Sharma[1]*, Ravi Chakra Turaga[1]*, Yi Yuan[1], Ganesh Satyanarayana[1], Falguni Mishra[1], Zhen Bian[1], Wei Liu[1,2], Li Sun[3], Jenny Yang[4], and Zhi-Ren Liu[1]

Fibrotic tumor stroma plays an important role in facilitating triple-negative breast cancer (TNBC) progression and chemotherapeutic resistance. We previously reported a rationally designed protein (ProAgio) that targets integrin $\alpha_v\beta_3$ at a novel site. ProAgio induces apoptosis via the integrin. Cancer-associated fibroblasts (CAFs) and angiogenic endothelial cells (aECs) in TNBC tumor express high levels of integrin $\alpha_v\beta_3$. ProAgio effectively induces apoptosis in CAFs and aECs. The depletion of CAFs by ProAgio reduces intratumoral collagen and decreases growth factors released from CAFs in the tumor, resulting in decreased cancer cell proliferation and apoptotic resistance. ProAgio also eliminates leaky tumor angiogenic vessels, which consequently reduces tumor hypoxia and improves drug delivery. The depletion of CAFs and reduction in hypoxia by ProAgio decreases lysyl oxidase (LOX) secretion, which may play a role in the reduction of metastasis. ProAgio stand-alone or in combination with a chemotherapeutic agent provides survival benefit in TNBC murine models, highlighting the therapeutic potential of ProAgio as a treatment strategy.

Introduction

Triple-negative breast cancer (TNBC), the most deadly form of breast cancer, is characterized by the absence of estrogen (ER) and progesterone (PR) hormone receptors and the lack of human epidermal growth factor 2 (HER2) expression. TNBC patients are at high risk of locoregional or distant recurrence, poor prognosis, and low overall survival (Haffty et al., 2006; O'Shaughnessy et al., 2011). In fact, TNBC patients with metastatic disease have a poorer prognosis, with a median survival of ~1 yr (O'Shaughnessy et al., 2011). There are very limited targeted therapies available for TNBC, and the treatment option is broadly cytotoxic chemotherapy drugs, despite their low efficacy and strong unwanted side effects (Cleator et al., 2007). Previous studies have highlighted the significance of the tumor microenvironment (TME) in mediating TNBC progression and affecting treatment efficacy (Dias et al., 2019; Sahai et al., 2020). It is noteworthy that the presence of abundant stroma in the patient tumor has a poorer outcome than with low stroma in the breast tumor in TNBC (de Kruijf et al., 2011; Moorman et al., 2012).

Cancer-associated fibroblasts (CAFs) are the most prominent cell types in the TME of TNBC, which actively engage in crosstalk with the surrounding cells, promoting cancer cell proliferation and survival. The interaction between CAFs and cancer cells is through excessive production of growth factors (GFs), chemokines, and cytokines. Additionally, CAFs secrete excessive extracellular matrix (ECM) proteins, particularly collagen and fibronectin, both of which initiate angiogenesis in the tumor (LeBleu and Kalluri, 2018; Neve et al., 2014; Zhou et al., 2008). Dense collagen secretion by CAFs impedes drug delivery and decreases drug uptake in solid tumors, which contributes to drug resistance (Baumgartner et al., 1998). CAFs in the tumor are heterogeneous. The subtypes of CAFs play a distinct role in cancer development and progression, sometimes completely opposite functions (Huelsken and Hanahan, 2018; Öhlund et al., 2014; Öhlund et al., 2017). The subsets of CAFs often express distinct gene signatures and secrete a distinct profile of soluble factors (e.g., GFs and cytokines), which enable its unique pro- or anti-cancer roles (Sahai et al., 2020; Su et al., 2018). Furthermore, CAF subfamilies may undergo constant changes orchestrated by dynamic CAF–cancer cell interactions (Sahai et al., 2020), which adds another layer of complexity to the functional role(s) of CAFs in cancer progression.

[1]Department of Biology, Georgia State University, Atlanta, GA; [2]Harbin Medical University Cancer Hospital, Harbin, People's Republic of China; [3]Amoytop Biotech Inc., Xiamen, People's Republic of China; [4]Department of Chemistry, Georgia State University, Atlanta, GA.

*M. Sharma and R.C. Turaga contributed equally to this paper; Correspondence to Zhi-Ren Liu: zliu8@gsu.edu.

The microvasculature in tumors of TNBC and basal-like breast cancer is denser than that of non-TNBC and non–basal-like breast cancer (Mohammed et al., 2011; Ribatti et al., 2016), indicating high angiogenic activity in TNBC and basal-like breast cancer. Furthermore, dense tumor microvasculature closely correlates with shorter recurrence-free survival and overall survival. Dense tumor vasculature is associated with a shorter time from diagnosis to relapse and from relapse to death (Linderholm et al., 2009). The dysregulated vessel structure in a TNBC tumor often leads to resistance to blood flow into the tumor, which is another important barrier for drug delivery. Interestingly, activation of fibroblasts and intratumoral angiogenesis is tightly coupled in the tumor. CAFs secrete a number of molecular factors that promote angiogenic endothelial cell (aEC) growth and migration (LeBleu and Kalluri, 2018; Mayrand et al., 2012; Wang et al., 2019), thus facilitating tumoral angiogenesis, while aECs also play a role in maintaining CAF activation (Lopes-Bastos et al., 2016; Relf et al., 1997). In addition, the ECM that is released by CAFs also plays a role in promoting intratumoral angiogenesis (Sewell-Loftin et al., 2017; Vong and Kalluri, 2011).

Both CAFs and tumor angiogenesis have been implicated as primary mediators of cancer cell dissemination to distant sites. Intratumoral hypoxia induces CAFs and cancer cells to secrete an enzyme lysyl oxidase (LOX), which cross-links and stabilizes ECM components, particularly collagen, present in abundance in the TME of breast tumors. The stiffer microenvironment at the primary tumor site forms ECM tracks to assist cancer cell migration and therefore metastases (Emon et al., 2018). In addition, secretion of LOX promotes collagen remodeling at the metastatic site that facilitates bone marrow–derived cell accumulation, subsequently promoting cancer cell colonization at a secondary site (Wong et al., 2011). Overall, CAF and angiogenesis cooperatively play an important role in TNBC growth, survival, metastasis, and drug resistance. Therefore, simultaneously targeting CAFs and angiogenic vessels in TNBC could be a promising therapeutic strategy.

Both aECs and CAFs in breast cancer express high levels of integrin $\alpha_v\beta_3$ (Attieh et al., 2017; Brooks et al., 1994). We previously reported a rationally designed protein, ProAgio, that targets integrin $\alpha_v\beta_3$ at a novel site and induces apoptosis in the integrin-expressing cells by recruiting caspase 8 at the cytoplasmic domain of β_3 (Turaga et al., 2016). We report here that ProAgio induces apoptosis in integrin $\alpha_v\beta_3$–expressing CAFs and aECs in TNBC. Depletion of CAFs by ProAgio decreases intratumoral collagen. Depletion of CAFs by ProAgio reduces platelet-derived growth factor (PDGF), epidermal growth factor (EGF), and IGF1 levels in the tumor, abrogating CAF and cancer cell crosstalk, which consequentially decreases tumor growth and cancer cell apoptosis resistance. Depletion of CAFs by ProAgio also reduces LOX levels in the tumor and blood circulation. Reduction of LOX may play a role in reducing cancer metastasis. In addition, the anti-angiogenesis effect of ProAgio eliminates angiogenic leaky tumor vessels, which consequently facilitates drug delivery and decreases hypoxia in murine models of TNBC. Furthermore, depletion of CAFs by ProAgio at metastatic sites decreases collagen and LOX at metastatic sites, which reduces

cancer cell colonization by preventing the formation of a pre-metastatic niche. Depletion of CAFs at the metastatic site by ProAgio may also inhibit metastatic tumor growth. ProAgio, stand-alone or in combination with other chemotherapeutic agents, demonstrates high anti-tumor efficacy and prolonged survival of tumor-bearing mice, suggesting an excellent treatment strategy for TNBC, especially for poor-prognosis patients with high tumor stroma.

Results

Abundant stroma rich in integrin $\alpha_v\beta_3$-expressing CAFs and collagen is associated with poor TNBC patient survival

TNBC patients with stroma-rich tumors have a higher risk of relapse and treatment resistance and lower overall survival compared with patients with low-stroma tumors (de Kruijf et al., 2011; Moorman et al., 2012). We first analyzed the tumor sections of TNBC patients for the abundance of stroma. H&E staining demonstrated both high and low amounts of stroma in TNBC patient tumor sections (Fig. 1 A). We next performed Sirius red staining for collagen and immunostaining for α–smooth muscle actin (α-SMA) and fibroblast activation protein (FAP) and observed both high and low expressions of collagen, α-SMA, and FAP-positive cells in the tumors of TNBC patients (Fig. 1 A). We then analyzed survival of TNBC patients with high and low gene expression of collagen (COL1A1, COL1A2) and FAP (CAF) from a publicly available dataset obtained from cbioportal (http://www.cbioportal.org). Consistent with previous studies, a high amount of collagen and FAP correlates with poor survival in TNBC patients (Fig. 1, B and C; and Fig. S1, A–D).

Previous studies have reported the expression of integrin $\alpha_v\beta_3$ in CAFs (Attieh et al., 2017). We evaluated integrin $\alpha_v\beta_3$ expression in breast cancer CAFs in the tumors of TNBC patients. Immunohistochemistry (IHC) staining of integrin β_3 demonstrated that the integrin was highly upregulated in the histologically evident stromal component of the tumors (Fig. 1 D). To verify the expression of integrin in breast cancer CAFs, we first assessed whether the integrin is expressed in human mammary fibroblasts (hMFs) upon TGF-β activation. Immunoblotting revealed that integrin $\alpha_v\beta_3$ was highly expressed in activated hMFs but not in nonactivated hMFs (Fig. 1 E). Immunofluorescence costaining (Co-IF) of integrin β_3 with α-SMA in activated hMFs also demonstrated the expression of the integrin in the activated fibroblasts. Murine CAFs were isolated from orthotopic 4T1 tumors. Co-IF staining revealed that integrin β_3 was highly expressed in α-SMA–positive murine CAFs (Fig. 1 F). Expression of the integrin β_3 in fibroblasts isolated from tumors of breast cancer patients (referred to as hbCAFs) was verified by immunoblotting (Fig. S1 E). Integrin expression in CAFs was further verified by Co-IF staining of integrin β_3 and α-SMA in 4T1 tumor sections (Fig. S1 F). Additionally, cells from MMTV-PyMT breast tumor tissue were sorted using magnetic-assisted cell separation (MACS) technique followed by RT-PCR analysis for cell characterization. The mRNA analysis revealed a high expression of integrin $\alpha_v\beta_3$ in CAFs and endothelial cells in the MMTV-PyMT breast tumor tissue (Fig. S1, G–I). Furthermore, patient survival data showed
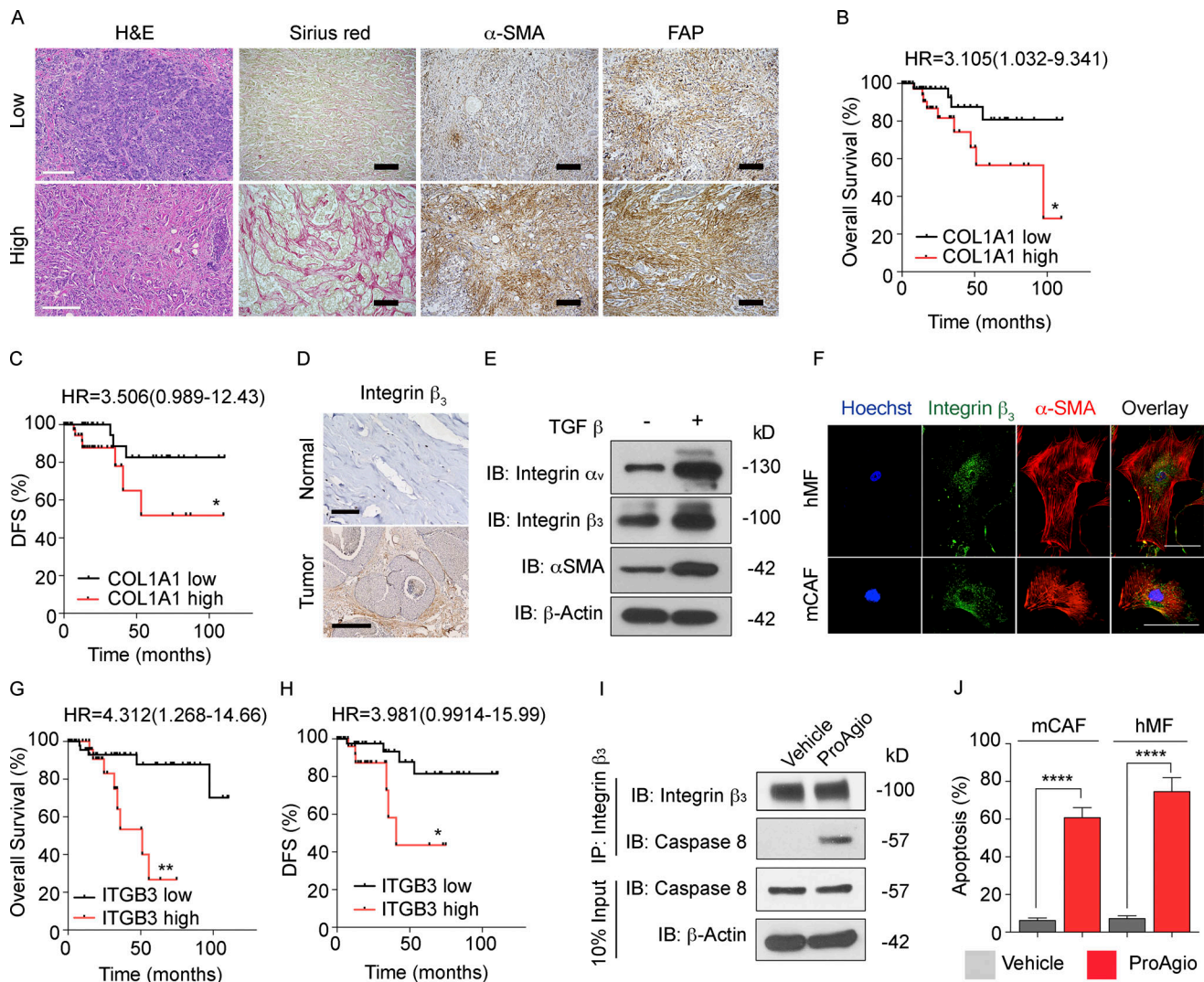
Sharma et al.
A novel treatment strategy for TNBC

Journal of Experimental Medicine 2 of 20
https://doi.org/10.1084/jem.20200712

Figure 1. **Abundant stroma rich in integrin $\alpha_V\beta_3$-expressing CAFs and collagen is associated with poor TNBC patient survival. (A)** Representative images of H&E staining, Sirius red staining, α-SMA, and FAP IHC staining of low stroma (upper panel) and high stroma (lower panel) in the breast tumors of TNBC patients ($n = 80$). Scale bars, 200 μm. **(B and C)** Kaplan-Meier overall survival (B) and DFS (C) analyses of low and high COL1A1 expression (COL1A1 low, $n = 44$; COL1A1 high, $n = 38$) in the tumors of TNBC patients. **(D)** Representative images of IHC staining of integrin β_3 in the breast tumor of TNBC patients (lower panel, $n = 80$; scale bar, 500 μm) compared with adjacent normal breast tissue (upper panel, $n = 3$; scale bar, 100 μm). **(E)** Levels of integrin α_V (IB: Integrin α_V), integrin β_3 (IB: Integrin β_3), and α-SMA (IB: α-SMA) in the nonactivated (−TGF-β) and activated (+TGF-β) hMFs were analyzed by immunoblot. hMFs were activated by culturing for 48 h in the presence of 5 ng/ml TGF-β. Nonactivated hMFs are the cells that are cultured for 1 d without TGF-β. **(F)** Representative Co-IF images of integrin β_3 (green) and α-SMA (red) in activated hMFs (upper panel) and murine CAFs (lower panel). Nuclei were counterstained with Hoechst (blue). Scale bars, 100 μm. **(G and H)** Kaplan-Meier overall survival analyses (G) of ITGB3 (integrin β_3: low, $n = 50$; high, $n = 32$) and DFS analyses (H) of ITGB3 (integrin β_3: low, $n = 45$; high, $n = 30$) in the tumors of TNBC patients. **(I)** Co-immunoprecipitation (coIP) of caspase 8 with integrin β_3 (IP: Integrin β_3) was analyzed by immunoblot (IB: caspase 8). Activated hMFs were treated with 5 μM ProAgio for 3 h. Immunoblot of integrin β_3 (IB: Integrin β_3) indicates the amount of β_3 that was coprecipitated down in the coIP. Input represents 10% of the total protein used for IP. **(J)** Apoptosis in murine CAFs (left panel) and activated hMFs (right panel) that were treated with 5 μM ProAgio (red bar) compared with vehicle (PBS, gray bar) was analyzed by apoptosis kit. TCGA dataset of TNBC patients was obtained from cbioportal (https://www.cbioportal.org). HR, hazard ratio. Immunoblot of β-actin (IB: β-actin) in E and I is a loading control. Experiments were performed at least in triplicate. Error bars in J represent mean ± SEM. *, $P < 0.05$; **, $P < 0.01$; ****, $P < 0.0001$ by log-rank test (B, C, G, and H) or unpaired Student's t test (J).

that high and low integrin β_3 (ITGB3) expression correlates with patient survival in TNBC (Fig. 1, G and H). The examination of integrin β_3, α-SMA, and FAP levels in TNBC patient tissue samples revealed a close correlation, suggesting expression of integrin β_3 in CAFs (Fig. S1 J). Altogether, our data suggest that high levels of $\alpha_V\beta_3$-expressing CAFs and collagen are associated with poor prognosis in TNBC patients.

Depletion of CAFs by ProAgio decreases tumor growth and metastasis and prolongs tumor-bearing mice survival

We previously reported that the rationally designed protein ProAgio induces apoptosis in integrin $\alpha_V\beta_3$-expressing cells (Turaga et al., 2016). We reasoned that ProAgio would be effective in inducing apoptosis in breast cancer CAFs. Apoptosis assay showed that ProAgio effectively induced apoptosis in

hMFs activated by TGF-β by recruiting caspase 8 to the intracellular domain of β_3 (Fig. 1, I and J), while it had no effect on nonactivated hMFs (Fig. S1 K). Similarly, ProAgio also effectively induced apoptosis in CAFs isolated from 4T1 tumor (Fig. 1 J) and hbCAFs (Fig. S1, L and M). Furthermore, Co-IF of vinculin and actin in the activated hMFs showed that actin filament stress fibers and focal adhesion complex diminished upon ProAgio treatment (Fig. S1 N), indicating the loss of integrin $\alpha_v\beta_3$-mediated focal points. Integrin $\alpha_v\beta_3$ is expressed in highly metastatic breast cancer cells, especially bone metastatic cancer cells (Havaki et al., 2007; Liapis et al., 1996).

To test whether ProAgio also affects breast cancer cells via integrin $\alpha_v\beta_3$, we examined integrin $\alpha_v\beta_3$ expression in several TNBC cell lines. Immunoblot analyses showed different integrin expression patterns in different TNBC cell lines (Fig. S2 A). ProAgio did not affect the cell viability of these TNBC cells, although integrin $\alpha_v\beta_3$ is expressed in MDA-MB-468 (Fig. S2 B). We do not fully understand why ProAgio did not induce apoptosis in integrin $\alpha_v\beta_3$-expressing cancer cells. Resistance to caspase 8–mediated apoptosis may be one of the reasons.

To test whether ProAgio indeed acts on CAFs in tumors, we employed three breast cancer mouse models. 4T1 murine breast cancer cells were orthotopically implanted into the mammary gland of syngeneic Balb/c mice. MDA-MB-231 cells were orthotopically implanted in the mammary gland of nude mice. Cancer cells in these models do not express ER and PR, along with low HER2 expression (Foulkes et al., 2010). In addition, we also employed a genetically engineered mouse MMTV-PyMT model. Tumors in this genetically engineered mouse model are ER and PR negative and gradually lose HER2 expression at the late stage (Christenson et al., 2017). Tumors in all three models contain dense fibrotic stroma with abundant collagen fibers. Hence, these murine models are suitable to analyze the effects of ProAgio on CAFs and the effects of modulation of fibroblasts on the progression of the tumor (Calvo et al., 2013; Zhang et al., 2013). In the 4T1 model, ProAgio treatment was started after the tumor volume reached around 250 mm³, while in the MDA-MB-231 model, the treatment was started after the tumor volume reached around 150 mm³. In the MMTV-PyMT model, the treatment was initiated at 75 d of age. Mice bearing 4T1 and MDA-MB-231 tumors were administered 12 i.p. doses of ProAgio (10 mg/kg, based on our previous concentration-dependent efficacy analysis; Fig. 2, A and B; Turaga et al., 2016). Due to rapid tumor progression and increased overall tumor burden, dosage and doses of ProAgio were increased (15 daily i.p., 20 mg/kg) in the MMTV-PyMT mice (Fig. 2 K).

ProAgio significantly prolonged the survival (P < 0.0001) of 4T1 mice compared with the vehicle-treated group (Fig. 2 C). Consistently, ProAgio treatment inhibited tumor growth and reduced tumor weight (P < 0.001) compared with the vehicle-treated group (Fig. 2, D–F). Similarly, a significant increase in survival and a reduction in tumor volume/burden and tumor weight were observed in MDA-MB-231 mice (Fig. 2, G–J) and MMTV-PyMT mice upon ProAgio treatment (Fig. 2, L–O). Concomitant reduction in the tumor proliferation marker Ki67 (Fig. S2, C–F; also see Fig. 9 C) was observed in the tumors of all ProAgio-treated mice. Co-IF staining of Ki67 and pancytokeratin,

an epithelial cell marker, revealed that cancer cell proliferation was significantly reduced in ProAgio-treated 4T1 tumors (Fig. S2, G and H).

We next analyzed the effects of ProAgio on tumor stroma and CAFs. Sections from tumors of the treated mice were stained with α-SMA for CAFs and Sirius red for collagen. ProAgio-treated tumors exhibited markedly reduced α-SMA–positive cells and intratumoral collagen compared with the vehicle-treated mice (Fig. 3, A–H; also see Fig. 9, A and B). mRNA levels of α-SMA and FAP in the 4T1 tumors were analyzed by quantitative RT-PCR (qRT-PCR). Consistently, decreased α-SMA and FAP mRNA levels were observed in mice bearing a 4T1 tumor treated with ProAgio when compared with the vehicle group (Fig. S2 I). To verify that ProAgio indeed induces apoptosis in CAFs, we performed Co-IF staining of α-SMA and cleaved-caspase 3 (CC3) with sections from 4T1 tumors. Clearly, a significantly higher costain was observed in ProAgio-treated tumors than in the vehicle-treated group (Fig. 3, I–K). In addition, to determine whether ProAgio mediated apoptosis in cancer cells, we performed three-color IF staining with pancytokeratin, α-SMA, and CC3. A smaller increase in pancytokeratin and CC3 costaining compared with α-SMA and CC3 costaining indicated that although cancer cell apoptosis was higher in the ProAgio-treated 4T1 tumors as compared with the vehicle group, ProAgio induced more CAF apoptosis (Fig. S2, J and K). Further, immunoblot analysis of 4T1 breast tumor lysates verified that ProAgio treatment increased the levels of CC3 and cleaved-caspase 8 (CC8) compared with the vehicle group (Fig. S2 L). Thus, our experiments revealed that ProAgio inhibits tumor growth and prolongs survival of tumor-bearing mice by inducing apoptosis in breast cancer CAFs. Apoptosis in CAFs induced by ProAgio also consequentially increased apoptosis in cancer cells.

An important cancer-promoting role of CAFs is that CAFs engage in a symbiotic crosstalk with cancer cells that supports cancer cell growth, metastasis, and resistance to apoptosis. CAFs secrete GFs such as PDGF, EGF, and IGF1 in tumors, which promote cancer progression (LeBleu and Kalluri, 2018). Because ProAgio depletes CAFs, we reasoned that ProAgio would reduce intratumoral GFs and consequently decrease activation of GF receptors in cancer cells. We first analyzed the levels of PDGF, EGF, and IGF1 in primary 4T1 tumors by immunostaining and ELISA. Clearly, ProAgio decreased intratumoral PDGF, EGF, and IGF1 in the tumors (Fig. S3, A–C). We then examined phosphorylation of PDGFRβ, EGFR, IGF1R, and downstream targets, including Akt and ERK, in the sections of treated tumors by immunostaining. The ProAgio-treated 4T1 tumors had reduced activation of the aforementioned GF receptors and their downstream target molecules (Fig. S3, D and E). Secretion of GFs by CAFs activates GF receptors that mediate apoptotic resistance in cancer cells (Antonyak et al., 2004; Fingas et al., 2011).

We cultured TNBC cells, MDA-MB-231, 4T1, BT549, and HCC1806 with the GF cocktail (PDGF, EGF, IGF1, and hepatocyte GF) and subsequently treated them with different concentrations of chemotherapeutics, paclitaxel (PTX) and doxorubicin (DOX). Clearly, addition of GFs increased viability of all the TNBC cells (Fig. S3, F–K). Furthermore, we cultured MDA-MB-231 and 4T1
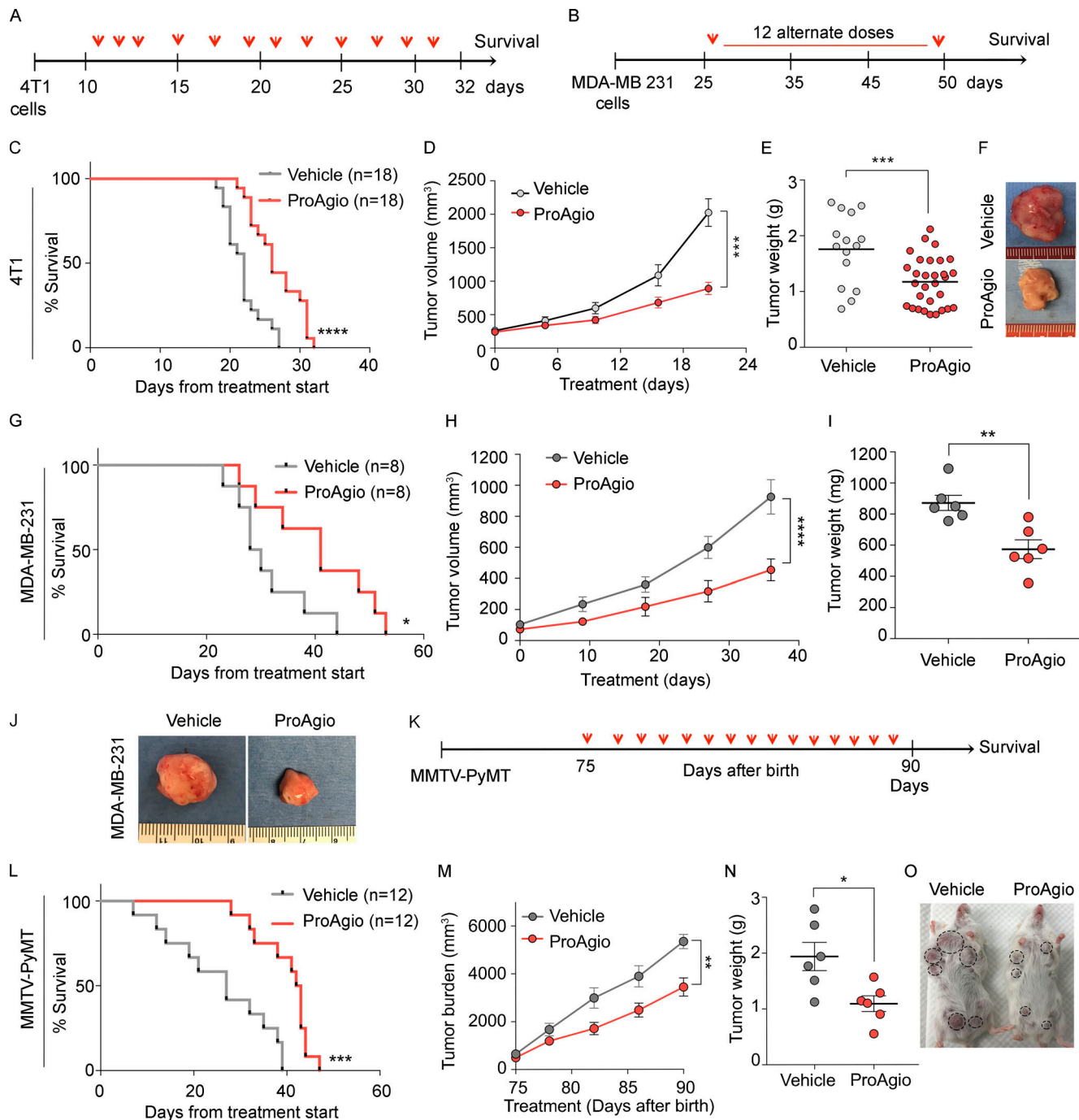
Figure 2. **ProAgio reduces breast tumor growth and prolongs survival in tumor-bearing mice. (A and B)** Therapy regimen of ProAgio (i.p.; indicated by red arrows) in 4T1 (A) and MDA-MB-231 (B) mice. **(C–F)** Kaplan-Meier survival analysis (*n* = 18; median survival: vehicle, 22 d; ProAgio, 26 d; C), mean tumor volume (D), mean tumor weight (E), and representative images of tumor (F) of 4T1 tumor-bearing mice treated with vehicle or ProAgio (vehicle, *n* = 15; ProAgio, *n* = 30). **(G–J)** Kaplan-Meier survival analysis (*n* = 8; median survival: vehicle, 29 d, ProAgio, 41 d; G), mean tumor volume (*n* = 10; H), mean tumor weight (*n* = 6; I), and gross images of breast tumor (J) of MDA-MB-231 female nude mice treated with vehicle or ProAgio. **(K)** Therapy regimen of 20 mg/kg ProAgio (i.p.; indicated by red arrows) in MMTV-PyMT mice. **(L–O)** Kaplan-Meier survival analysis (*n* = 12; median survival: vehicle, 27 d; ProAgio, 42.5 d; L), mean tumor burden (*n* = 12; M), average tumor weight (*n* = 6; N), and representative images showing gross appearance of tumors where dotted lines demarcate tumor masses (O) of MMTV-PyMT mice treated with vehicle or ProAgio. Error bars represent mean ± SEM. *, P < 0.05; **, P < 0.01; ***, P < 0.001; ****, P < 0.0001 by unpaired Student's *t* test.

cells with the conditioned medium from mammary CAFs. Consistently, an increase in cell viability was observed upon treatment with DOX (Fig. S3, L and M). The results suggest that conditioned medium from CAFs or GFs conferred chemoresistance in TNBC cells.

To verify whether a decrease in GFs due to depletion of CAFs by ProAgio sensitizes cancer cells to apoptosis induction, we cultured mammary fibroblasts with MDA-MB-231 cells in a Boyden chamber that mimics the co-culture (Fig. S3 N). We first
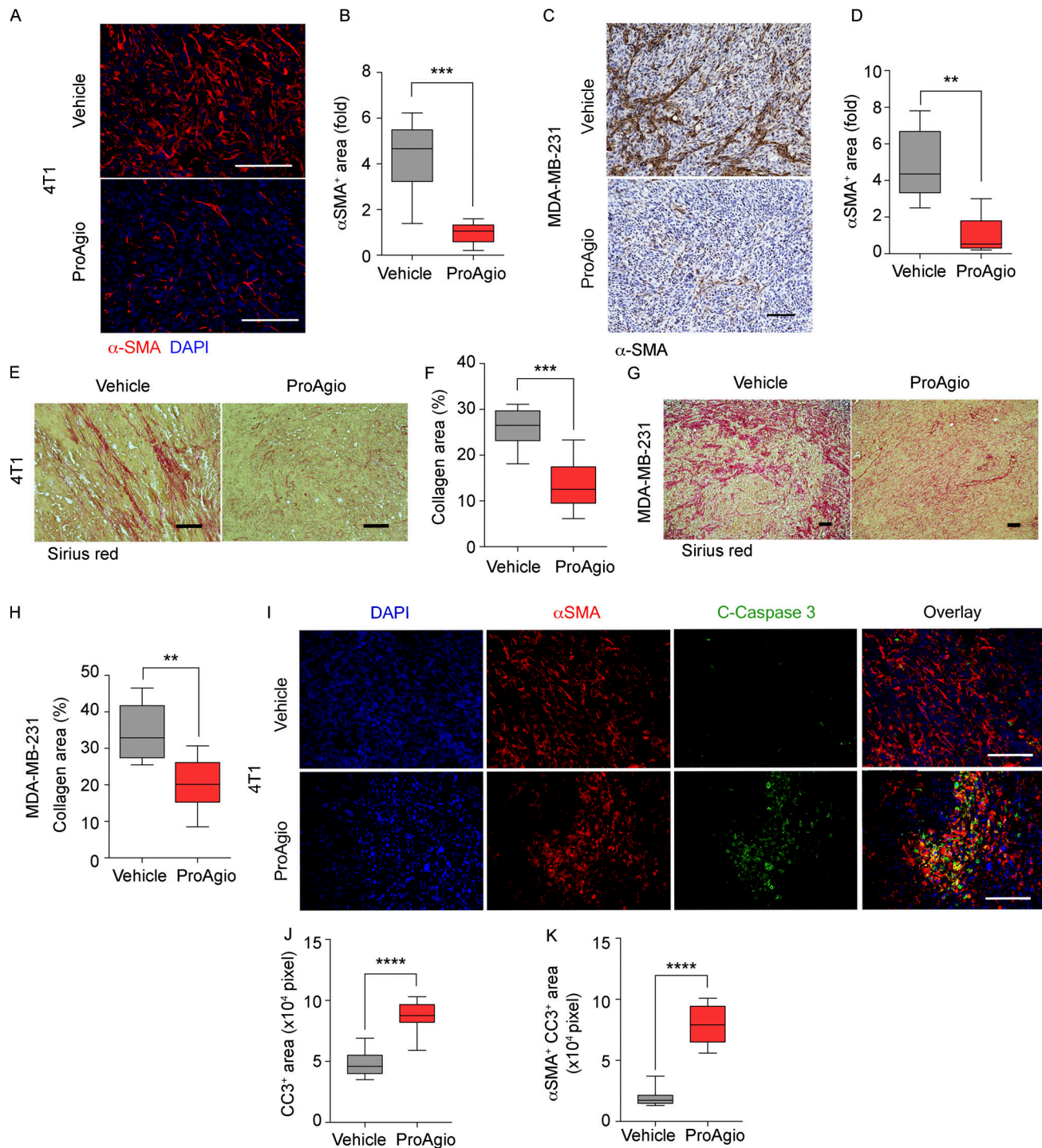
Figure 3. **ProAgio decreases CAFs and collagen in TNBC mouse models by inducing apoptosis in breast cancer CAFs. (A and B)** Representative images of IF staining of α-SMA (A) and quantification of α-SMA⁺ area (B) in the tumors of 4T1 mice treated with vehicle or ProAgio; n = 6/group. Scale bars, 100 μm. **(C and D)** Representative images of IHC staining of α-SMA (C) and quantification of α-SMA⁺ area (D) in the tumors of MDA-MB-231 mice treated with vehicle or ProAgio; n = 6/group. Scale bar, 100 μm. **(E and F)** Representative images of Sirius red staining (E) and quantification of collagen area (F) in the tumors of 4T1 mice treated with vehicle or ProAgio; n = 7/group. Scale bars, 100 μm. **(G and H)** Representative images of Sirius red staining (G) and quantification of collagen area (H) in the tumors of MDA-MB-231 mice treated with vehicle or ProAgio; n = 6/group. Scale bars, 100 μm. **(I–K)** Representative images of IF costaining of α-SMA (red) and CC3 (green; I), quantification of apoptotic cells (CC3⁺ area; J), and apoptotic breast cancer CAFs (α-SMA⁺ CC3⁺ area; K) in tumor sections of 4T1 mice treated with vehicle or ProAgio. Nuclei were counterstained with DAPI (blue); n = 5–6/group. Scale bars, 100 μm. **, P < 0.01; ***, P < 0.001; ****, P < 0.0001 by unpaired Student's t test.

treated MFs with vehicle or ProAgio for 6 h and thereafter treated with DOX. Immunoblot analysis demonstrated that ProAgio treatment decreased phospho-ERK (pERK) and phospho-Akt (pAkt) in MDA-MB-231 cells (Fig. S3 O). DOX induced higher levels of apoptosis in MDA-MB-231 cells in the presence of ProAgio (Fig. S3 P), suggesting that depletion of CAFs by ProAgio sensitizes cancer cells to apoptosis induction.

ProAgio reduces TNBC metastasis by modulating fibrotic stroma at both primary and metastatic sites

The lung is one of the major metastatic organ sites in breast cancer patients, especially in TNBC, as the incidence of lung metastasis is 40% in TNBC compared with 20% in non-TNBC (Foulkes et al., 2010). The lung is also the major metastatic site in orthotopic 4T1, orthotopic MDA-MB-231, and MMTV-PyMT mouse models (Jonkers and Derksen, 2007). It is well-known that CAFs play an important role in promoting cancer cell metastasis (Quail and Joyce, 2013). Since ProAgio depletes CAFs in breast tumors, we reasoned whether ProAgio would have effects on metastasis. We analyzed the effects of ProAgio on lung metastasis in three models. ProAgio treatment reduced the number (Fig. 4, A and B; and Fig. S4, A and B) and the size of lung metastatic nodules in 4T1 and MDA-MB-231 mice (Fig. S4, C and D) and MMTV-PyMT mice (Fig. 4, C and D; and Fig. S4, E), suggesting that depletion of breast cancer CAFs reduces breast cancer metastasis.

ProAgio induced CAF apoptosis and reduced collagen content in the primary tumors of three tested breast cancer models. We asked whether ProAgio also exerted its effects on CAFs and collagen at the lung metastatic site. We analyzed CAFs and collagen in lung metastatic tumors in both 4T1 and MMTV-PyMT models. Metastatic tumors in the lung in ProAgio-treated animals displayed reduced α-SMA–positive cells (Fig. 4, E and F) and intratumoral collagen (Fig. 4, E and G) compared with vehicle-treated mice in both models. ProAgio treatment also led to an over-2.5-fold increase in costaining of α-SMA with CC3 in sections of 4T1 lung metastatic tumors (Fig. 4, H and I), suggesting that ProAgio induces lung CAF apoptosis in TNBC. We further validated the effect of ProAgio in the metastatic lung lysates of 4T1 mice by immunoblotting. ProAgio treatment resulted in increased CC3 and CC8 levels in the lung lysates of 4T1 mice (Fig. S4 F).

To verify the effects of ProAgio on lung CAFs, we examined expression of integrin $\alpha_v\beta_3$ and α-SMA in human lung fibroblasts (hLFs) upon activation with TGF-β. Evidently, TGF-β–activated hLFs express high levels of integrin $\alpha_v\beta_3$, α-SMA (Fig. 4 J and Fig. S4 G), and vimentin (Fig. S4 G); however, nonactivated hLFs did not express high levels of integrin $\alpha_v\beta_3$ (Fig. 4 J). Consistently, ProAgio effectively induced apoptosis in the activated hLF by recruiting caspase 8 to the intracellular domain of β_3 (Fig. S4, H and I), while it had no effect on the nonactivated hLF (Fig. S4 J).

To confirm the effects of ProAgio at lung metastatic sites, 4T1 cells were i.v. injected into Balb/c mice via the tail vein (spontaneous model). The mice were treated with ProAgio the next day after cancer cell injection for 12 daily doses (Fig. 4 K). Animals were sacrificed 3 d after ProAgio treatment. Tumor nodules

in the lung were analyzed. Clearly, ProAgio reduced both lung tumor nodule number (Fig. 4, L and M) and size (Fig. S4 K). Sirius red and α-SMA staining in the metastatic tumor sections demonstrated that ProAgio reduced α-SMA–positive CAFs (Fig. S4, L and M) and collagen in the tumors (Fig. S4, N and O). The results suggest that ProAgio decreases metastatic tumor colonization at metastatic sites due to the action on CAFs and the fibrotic stroma.

Eliminating angiogenic vessels by ProAgio increases blood perfusion into the tumor and enhances chemotherapeutic delivery and efficacy

Studies have shown that tumor angiogenesis leads to leaky tumor vessels, which impairs blood flow into and from the tumor, leading to hypoxia. The leaky vessels form a major barrier to drug delivery (Polydorou et al., 2017). We have previously demonstrated anti-angiogenesis activity of ProAgio due to induction of apoptosis in integrin $\alpha_v\beta_3$-expressing aECs (Turaga et al., 2016). A decrease in CD31 staining in 4T1 and MMTV-PyMT tumors in ProAgio-treated mice corroborated our previous findings (Fig. 5, A, B, E, and F). In addition, ProAgio-treated 4T1 mice displayed a decrease in number of branch points and vessel length in the breast tumor (Fig. 5, C and D).

We reasoned that removal of leaky angiogenic tumor vessels would improve blood perfusion into the tumor. To test this speculation, lectin perfusion assay (Park et al., 2016) was performed using fluorescent conjugated lectin in 4T1 mice at the end of ProAgio treatment. Clearly, lectin perfusion in the tumor was more than doubled in the ProAgio-treated mice compared with the vehicle-treated mice (Fig. 5, G and H). Vascular leakage was analyzed by dextran leakage assay (Park et al., 2016). Evidently, the intratumoral vessel leakage was decreased in the 4T1 tumor treated with ProAgio compared with the vehicle-treated group (Fig. 5, I and J). The results suggest that ProAgio decreases leaky vessels in tumors and increases tumor blood perfusion.

Removal of leaky blood vessels in the breast tumor would facilitate drug molecule delivery into the tumor, thus enhancing the efficacy of chemotherapy (Jain, 2005). ProAgio effectively depletes CAFs, reduces intratumoral collagen, and eliminates leaky tumor angiogenic vessels. It is therefore expected that ProAgio would facilitate drug delivery. To evaluate the effects of ProAgio on drug delivery, 4T1 mice were treated with 12 daily doses of ProAgio, followed by one i.v. dose of PTX. Tumor lysates were subsequently analyzed by HPLC. Intriguingly, ProAgio treatment resulted in an increase in intratumoral PTX in 4T1 mice (Fig. 5 K). The observation was further verified by analyzing delivery of the fluorescence probe–conjugated PTX to the tumors of 4T1 mice treated with vehicle or ProAgio (Fig. 5, L and M).

Removal of disorganized leaky tumor angiogenic vessels improves tumor blood flow and oxygenation, which consequently decreases tumor hypoxia (Jain, 2005). Therefore, we assessed whether ProAgio treatment altered tumor hypoxia in 4T1 and MMTV-PyMT tumors. Pimonidazole was i.v. administered in 4T1 mice. A significant decrease in hypoxyprobe-1 signal in ProAgio-treated mice was observed (Fig. 5, N and O). In addition, immunostaining analyses demonstrated that HIF-1α was
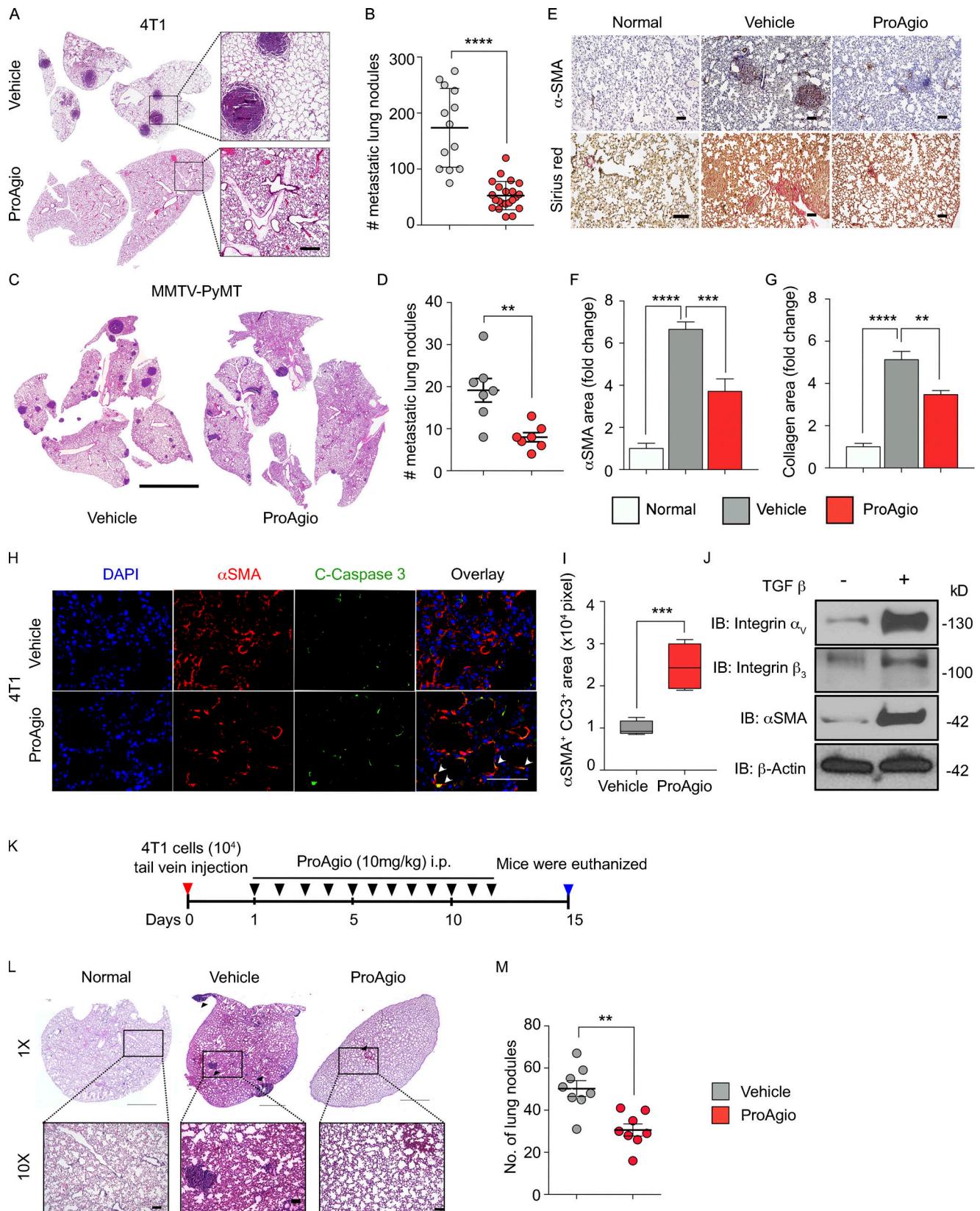
Sharma et al.
A novel treatment strategy for TNBC

Journal of Experimental Medicine   7 of 20
https://doi.org/10.1084/jem.20200712

Figure 4. **ProAgio reduces metastasis to the lungs by modulating fibrotic stroma at the lung metastatic site. (A and B)** Representative images of H&E staining of the lungs (A) and quantification of number of lung metastatic nodules (B) in tumor sections of 4T1 mice treated with vehicle or ProAgio (vehicle, *n* = 13; ProAgio, *n* = 22). Scale bar, 100 μm. **(C and D)** Representative images of H&E staining of the lungs (C) and quantification of the number of lung metastatic nodules (D) in tumor sections of MMTV-PyMT mice treated with vehicle or ProAgio. Scale bar, 4 mm. **(E–G)** Representative images of IHC staining of α-SMA

(upper panel) or Sirius red staining (lower panel; E) and quantification of α-SMA$^+$ area (F) and collagen area (G) in the sections of metastatic lungs of 4T1 mice treated with vehicle (gray bar) or ProAgio (red bar). Normal represents the lung sections from mice without a tumor and treatment (open bar); n = 8/group. Scale bars, 100 µm. **(H and I)** Representative images of Co-IF of α-SMA (red) and CC3 (C-caspase 3; green; H) and quantification of apoptotic α-SMA$^+$ CAFs (α-SMA$^+$ CC3$^+$ area; I) in the sections of metastatic lungs of 4T1 mice treated with vehicle or ProAgio. Nuclei were counterstained with DAPI (blue). White arrowheads indicate colocalization; n = 5/group. Scale bar, 100 µm. **(J)** Levels of integrin α$_V$ (IB: Integrin α$_V$), integrin β$_3$ (IB: Integrin β$_3$), and α-SMA (IB: α-SMA) in the nonactivated (−TGF-β) and activated (+TGF-β) hLFs were analyzed by immunoblot. hLFs were activated by culturing for 48 h in the presence of 5 ng/ml TGF-β. Nonactivated hLFs are the cells that are cultured for 1 d without TGF-β. β-actin is a loading control. Data are representative of at least three independent biological replicates. **(K)** Therapy regimen of the 4T1 spontaneous model. On day 15, the mice were sacrificed and the lungs were collected. **(L and M)** Representative images of H&E staining (L) and quantification of tumor nodules (M) in lung sections of the vehicle- or ProAgio-treated animals. Scale bars, top panel: 1,000 µm; lower panel: 100 µm. Error bars represent mean ± SEM. **, P < 0.01; ***, P < 0.001; ****, P < 0.0001 by unpaired Student's t test.

decreased in ProAgio-treated 4T1 and MMTV-PyMT tumors compared with the vehicle-treated group (Fig. 5, N–Q).

Reduction in LOX in tumors due to depletion of CAFs and decreased hypoxia by ProAgio may play a role in reducing cancer metastasis

LOX is an enzyme mediating lysine oxidation in the ECM, which helps the ECM, mostly collagen cross-linking, to enable metastasis progression. It is documented that hypoxia in tumors upregulates LOX expression and secretion in the cancer cells (Ji et al., 2013; Wong et al., 2011). We examined LOX expression in 4T1 and MDA-MB-231 cells under hypoxia and normoxia conditions. Consistent with observations made by other laboratories, hypoxia strongly increased LOX expression and secretion in cancer cells (Fig. 6, A and B). Myofibroblasts are the main source cells that secrete LOX during tissue repair and wound healing (Fushida-Takemura et al., 1996). CAFs share most of the characteristics with myofibroblasts (Kalluri, 2016). We therefore examined LOX expression in activated/nonactivated hMFs. Clearly, hMFs expressed high levels of LOX upon TGF-β activation (Fig. 6 C). Our results suggest that CAFs are another major source of LOX in breast tumors.

ProAgio depletes breast cancer CAFs and reduces tumor hypoxia due to the abrogation of tumor angiogenesis. We reasoned that ProAgio would decrease LOX expression and secretion in tumors and consequentially play a role in reducing TNBC metastasis. To test this speculation, we first analyzed LOX in the sections of primary 4T1 and MMTV-PyMT tumors by immunostaining. A significant reduction in LOX staining in ProAgio-treated tumors was observed (Fig. 6, D–G). We further analyzed mRNA levels of other LOX family members, including LOXL2 and LOXL4 in 4T1 tumors by qRT-PCR. ProAgio treatment led to reduced LOX, LOXL2, and LOXL4 mRNA levels in 4T1 tumors (Fig. 6, H and I). Our data clearly indicate that in addition to decreasing LOX, ProAgio also reduced other LOX family members, LOXL2 and LOXL4, that are associated with high invasive potential. Next, we measured LOX activity in 4T1 and MMTV-PyMT tumor lysates. ProAgio decreased LOX activity in both 4T1 and MMTV-PyMT tumor lysates (Fig. 6, J and K). As LOX facilitates collagen cross-linking, we analyzed collagen cross-links in tumor sections by polarized light microscopy on Sirius red staining. Clearly, ProAgio led to a reduction in cross-linked collagen compared with vehicle-treated 4T1 and MMTV-PyMT tumors (Fig. 6, L–O).

LOX creates a favorable milieu at the metastatic site for cancer cells to colonize. Consistently, it has been shown that LOX is important for premetastatic niche formation in

orthotopic 4T1 and MMTV-PyMT mouse models (Pickup et al., 2013; Rachman-Tzemah et al., 2017). LOX in the metastatic cancer site would first likely come from release of the enzymes by primary tumors into the blood circulation (Wong et al., 2012). Colonization and growth of the metastatic tumors would create a second source for more LOX accumulation at the metastatic site. CAFs in the metastatic tumor site may be one of the major sources of LOX secretion at the metastatic site (Pickup et al., 2013). Therefore, we asked whether ProAgio affects LOX levels in the blood circulation and at the metastatic tumor. We analyzed LOX levels in the serum of 4T1 and MMTV-PyMT mice by LOX activity assay. ProAgio treatment led to a significant decrease in serum levels of LOX in both 4T1 and MMTV-PyMT mice (Fig. 7, A and B). IHC analyses of sections of metastatic lung tumors also demonstrated approximately threefold and approximately fivefold decreases in LOX in 4T1 and MMTV-PyMT mice, respectively, upon ProAgio treatment (Fig. 7, C–F). These observations are consistent with the results of the primary tumor sections. Concomitantly, we found a significant decrease in cross-linked collagen in the lung metastatic tumors of ProAgio-treated 4T1 and MMTV-PyMT mice (Fig. 7, G–K).

LOX at the metastatic cancer site recruits CD11b-positive myeloid cells, which facilitates colonization of metastatic cancer cells (Wong et al., 2012). Because we observed a decrease in LOX levels in the lungs of 4T1 and MMTV-PyMT mice, we analyzed CD11b-positive myeloid cells gated on CD45$^+$ tumor-infiltrating leukocytes in the metastatic lungs by flow cytometry. Evidently, ProAgio decreased CD11b-positive myeloid cells in the lungs of both 4T1 and MMTV-PyMT mice (Fig. 7, L–O). Reduction in CD11b cells by ProAgio at the metastatic tumor site also supports the notion that depletion of CAFs at the metastatic site correlates with reduced cancer cell colonization at the metastatic site (Wong et al., 2012). Altogether, our data demonstrate that ProAgio modulates breast cancer TME by inducing apoptosis in CAFs, consequentially reducing levels of LOX both at primary and metastatic tumors, which correlates with reduced cancer cell colonization in the lungs. Further, we performed a retrospective study to examine the clinical relevance of LOX in women with TNBC using a publicly available dataset. High expression of LOX was closely associated with poor overall survival (Fig. 7, P and Q), suggesting a critical role of LOX in TNBC patients.

Simultaneous depletion of CAFs and angiogenic tumor vessels by ProAgio enhances the efficacy of chemotherapeutics

An increase in chemotherapy drug delivery in addition to a decrease in cancer cell proliferation and apoptosis resistance
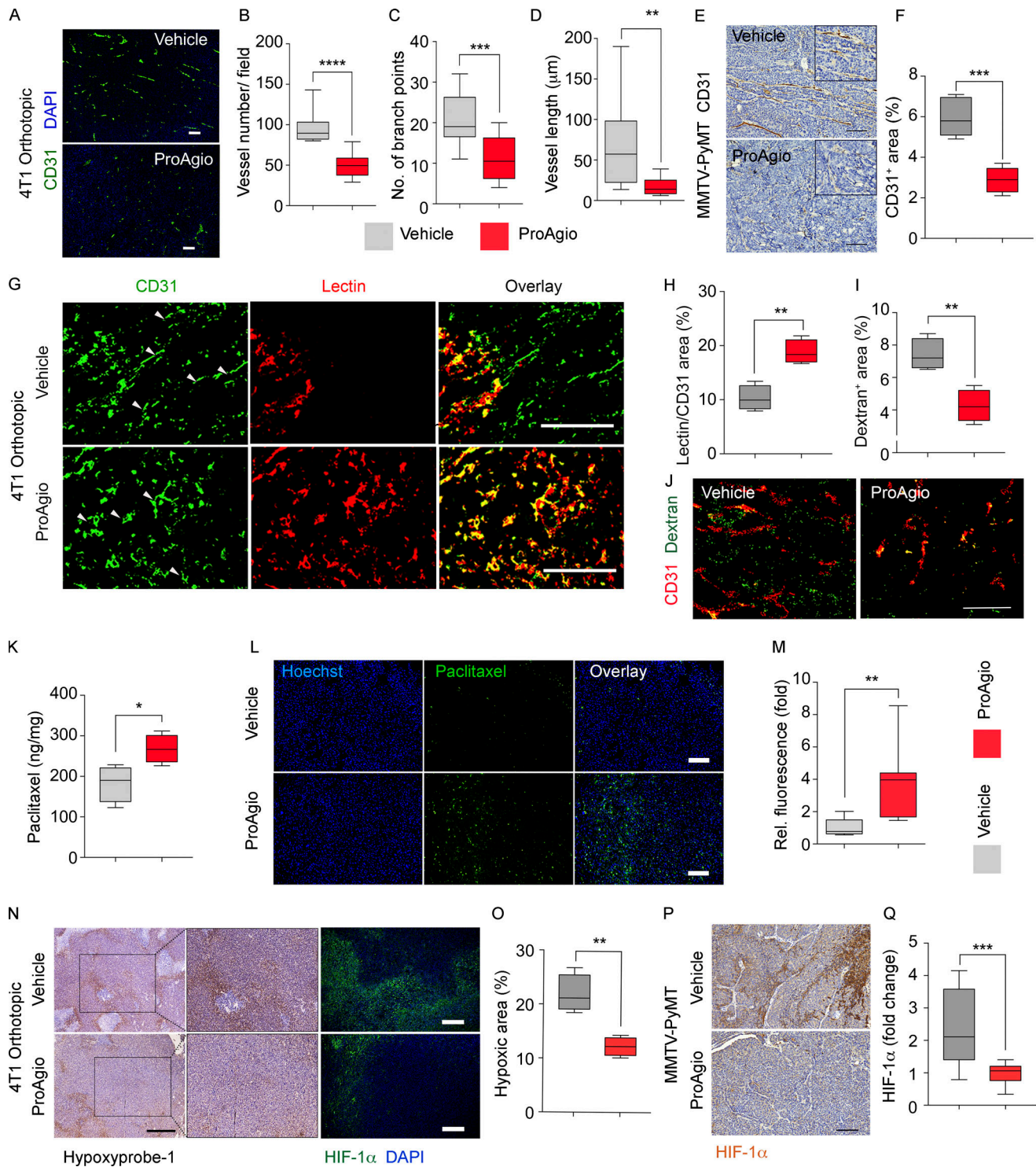
Figure 5. **ProAgio eliminates angiogenic vessels, enhances blood perfusion into the tumor, and consequentially reduces hypoxia. (A–D)** Representative images of IF CD31 staining (A), quantification of vessel number (B), number of branch points (C), and vessel length (D) per view field in tumor sections of 4T1 mice treated with vehicle or ProAgio. Nuclei were counterstained with DAPI (blue)**.** Scale bars, 100 µm (n = 6–7/group). **(E and F)** Representative IHC images of CD31 staining (E) and quantification of CD31+ area (F) in the breast tumor sections of MMTV-PyMT mice treated with vehicle or ProAgio. Insets, ×1.5. Scale bars, 100 µm (n = 5/group). **(G and H)** Representative fluorescence images of lectin perfusion in tumor vessels (G) and quantification of lectin-positive area (red) per total CD31-positive area (H; green, represented by white arrows) in tumor sections of 4T1 mice treated with vehicle or ProAgio. Scale bars, 100 µm (n = 4/group). **(I and J)** Representative IF images of dextran leakage of tumor vessels (J) and quantification of dextran+ area (I) in the breast tumor sections of 4T1 orthotopic mice. Dextran+ area is presented as a percentage per total section of the CD31+ area. Scale bar, 100 µm (n = 4/group). **(K)** Intratumoral levels of PTX in the extracts of tumors of 4T1 mice treated with vehicle or ProAgio. PTX levels were presented as nanograms of PTX per milligrams of tumor tissue (n = 4/group). **(L and M)** Representative fluorescence images of FITC-conjugated PTX (∼1 kD; L), and quantification of fluorescence signals (M) in the tumor sections of 4T1 mice treated with vehicle or ProAgio. Tumors were harvested at the end of the experiment (n = 3 or 4/group). Scale bars, 100 µm. **(N and O)**

Representative images of IHC staining of hypoxyprobe-1 (N, left panels; scale bar, 500 µm; $n = 4$/group) and IF staining of Hif-1α (N, right panels; scale bars, 200 µm; $n = 4$/group) and quantification of hypoxic area (O) in the tumor sections of 4T1 mice treated with vehicle or ProAgio. **(P and Q)** Representative images of IHC staining of HIF-1α (P) and quantitative analysis of HIF-1α (Q) in the breast tumors of MMTV-PyMT mice treated with vehicle or ProAgio. Scale bar, 100 µm. *, $P < 0.05$; **, $P < 0.01$; ***, $P < 0.001$; ****, $P < 0.0001$ by unpaired Student's t test.

due to reduction in intratumoral GFs would corroborate the synergistic effects of ProAgio in combination with chemotherapeutics. To test the hypothesis, 4T1 and MMTV-PyMT mice were treated with ProAgio and a low-dose PTX either alone or in combination. PTX alone did not have a significant effect on overall survival and tumor growth, while ProAgio alone provided survival benefit and inhibited tumor growth in the 4T1 mouse model. Interestingly, a low dose of PTX and ProAgio combination provided a significant survival benefit, inhibited tumor growth, and decreased end-point tumor weight (Fig. 8, A–E). Consistently, treatment of 4T1 mice with a combined regimen of ProAgio and a low dose of DOX significantly prolonged survival and decreased tumor growth and tumor weight (Fig. S5, A–E). Additionally, MMTV-PyMT mice also showed similar results upon treatment with a ProAgio and PTX combination. The combination therapy significantly increased overall survival and decreased total tumor volume and tumor volume of every nodule along with a decrease in total tumor weight (Fig. 8, F–I; and Fig. S5, F and G). Immunostaining of tumor sections with α-SMA and Sirius red staining for collagen revealed that ProAgio treatment alone decreased α-SMA and collagen; however, the combination of ProAgio + PTX further reduced α-SMA levels and collagen content compared with ProAgio. PTX alone had no significant effect on α-SMA levels and collagen content (Fig. 8, J and K). Also, the tumor proliferation marker Ki67 was dramatically reduced in the combination group (Fig. 9 A).

Next, analyses of the tumor tissues revealed an increase in apoptosis in the ProAgio + PTX group than ProAgio or PTX alone group in both 4T1 and MMTV-PyMT mice (Fig. S5, H and I; and Fig. 9 B). Consistently, an increase in apoptosis in the tumor with ProAgio + DOX combined therapy was observed in 4T1 mice (Fig. S5, H and I). Our data suggest that ProAgio increased the delivery of PTX/DOX, which led to an overall increase in apoptosis in the breast tumor. Examination of lung metastasis demonstrated that the ProAgio + PTX combination further reduced metastatic nodule number (Fig. S5, J and K; and Fig. 9, C–E). Altogether, our results indicate that ProAgio treatment conferred improved chemotherapeutic efficacy in the murine models by modulating breast cancer TME.

Discussion

CAFs are one of the main components of the TME. CAFs facilitate tumor progression through close crosstalk with cancer cells (LeBleu and Kalluri, 2018). Because of the cancer-promoting properties of CAFs, therapeutic strategies targeting tumor fibrotic stroma have been actively explored, particularly in the treatment of pancreatic ductal adenocarcinoma due to the unique properties of desmoplasia of pancreatic ductal adenocarcinoma. However, there is very limited success (Barnett and Vilar, 2018; Chen and Song, 2019). Although evidence has

demonstrated that dense fibrotic stroma closely correlates with poor prognosis in TNBC patients (de Kruijf et al., 2011; Moorman et al., 2012), targeting CAFs as a potential TNBC treatment has not been extensively explored (Takai et al., 2016). The angiogenic vessel is another important component of breast cancer TME. Tumor angiogenesis plays a critical role in promoting cancer progression (Carmeliet and Jain, 2000; Fox et al., 2007). Active angiogenesis in the tumor closely correlates with poor prognosis of patients with TNBC (Linderholm et al., 2009). It is well established that aECs express high levels of the integrin $\alpha_v\beta_3$ (Brooks et al., 1994). We demonstrate here that fibril-producing breast CAFs also express high levels of the integrin. We previously reported on ProAgio, a rationally designed protein that targets integrin $\alpha_v\beta_3$ at a novel site and specifically induces apoptosis in $\alpha_v\beta_3$-expressing cells (Turaga et al., 2016). The unique targeting specificity of ProAgio provides an effective approach to simultaneously deplete breast cancer CAFs and angiogenic tumor vessels (Fig. 9 F). Depletion of CAFs in TNBC tumors by ProAgio leads to a decrease in intratumoral collagen. Depletion of CAFs by ProAgio also reduces intratumoral GFs that are likely released by CAFs, which breaks down cancer-promoting CAF–cancer cell crosstalk.

LOX plays an important role in cancer metastasis (Rachman-Tzemah et al., 2017; Wong et al., 2011). Both cancer cells and CAFs secrete high levels of LOX. In the tumor with dense fibrotic stroma, CAFs may be the main source cells that secrete LOX (Pickup et al., 2013). Our data demonstrate that depletion of CAFs by ProAgio decreases LOX in the primary tumor, the blood circulation, and the metastatic site. Clearly, decreases in LOX both in the primary tumor and metastatic site may play a role in reducing TNBC metastasis, as shown in both 4T1 and MMTV-PyMT mouse models.

ProAgio also induces apoptosis in aECs in TNBC tumors and therefore diminishes the leaky tumor vasculature. Removal of dysregulated tumor angiogenic vessels increases blood perfusion into the tumor, which consequently improves drug delivery. Interestingly, an increase in blood perfusion into the tumor due to the abrogation of angiogenic tumor vessels by ProAgio not only facilitates drug molecule delivery but also reduces tumor hypoxia. Hypoxia is a critical regulatory factor in controlling the expression and secretion of LOX. Hypoxia is also one main driving force for cancer metastasis (Rankin and Giaccia, 2016). Interestingly, hypoxic CAFs promote tumor angiogenesis (Kugeratski et al., 2019). Simultaneous depletion of CAFs and angiogenic vessels in TNBC tumors by ProAgio leads to a decrease in the secretion of LOX by CAFs and a reduction in hypoxia, which also decreases hypoxia-driven LOX expression and secretion. Thus, it is clear that the dual actions of ProAgio in LOX expression/secretion and reduction in tumor hypoxia due to the anti-angiogenic activity of ProAgio orchestrate a special TME at both the primary and the metastatic tumor site to reduce
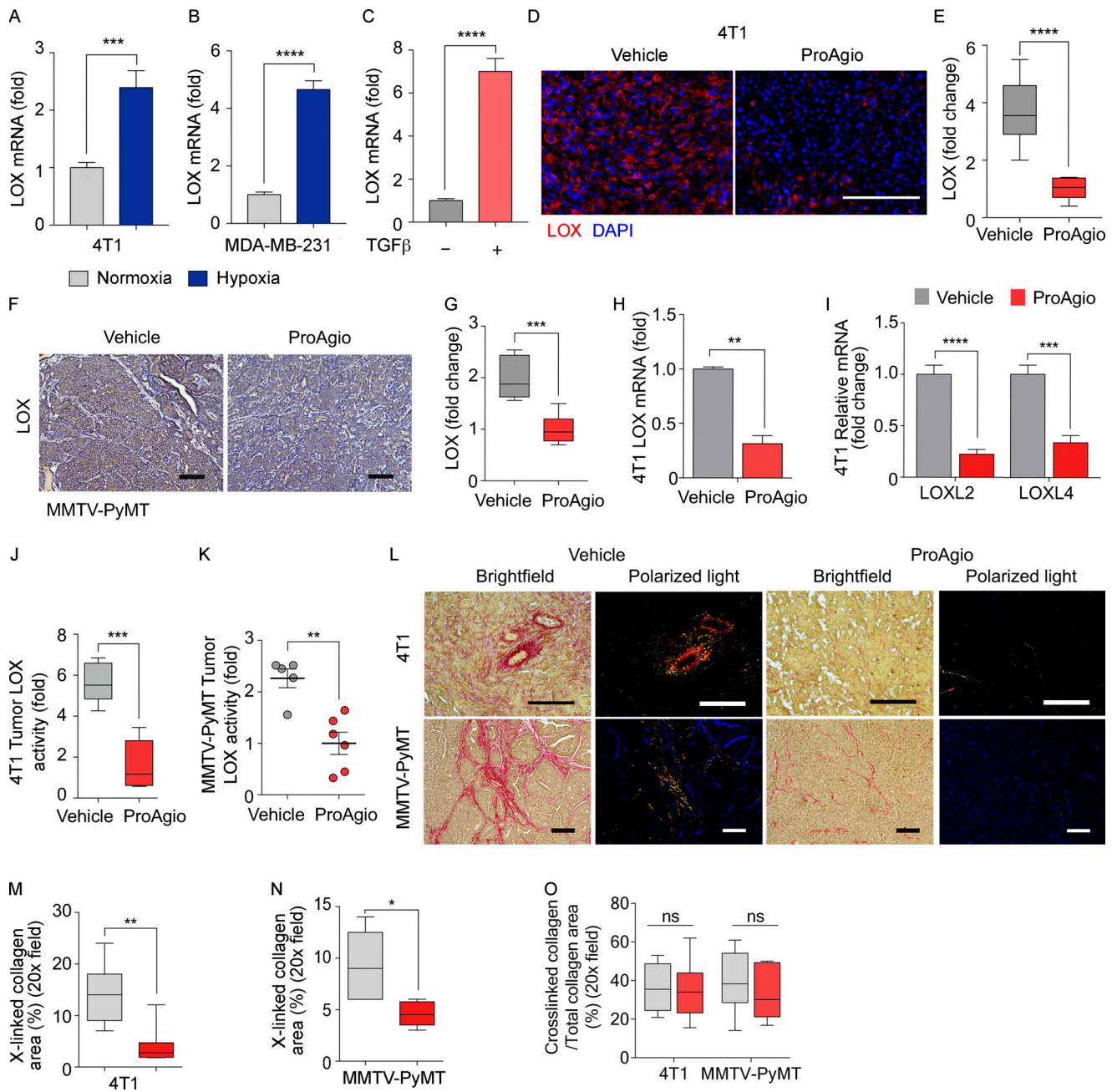
Sharma et al.
A novel treatment strategy for TNBC

Journal of Experimental Medicine   11 of 20
https://doi.org/10.1084/jem.20200712

Figure 6. **ProAgio decreases hypoxia-induced LOX secretion in the breast tumor in mouse models. (A–C)** Cellular levels of LOX mRNA in 4T1 cells (A), MDA-MB-231 cells (B) in normoxia (gray bar) or hypoxia (blue bar) condition, or hMFs nonactivated (−TGF-β, gray bar) or activated (+TGF-β, red bar) by TGF-β (C) were analyzed by qRT-PCR. All data are representative of at least three independent biological replicates. **(D and E)** Representative images of IF staining of LOX (D) and quantification of LOX staining (E) in the tumors of 4T1 mice treated with vehicle or ProAgio. Nuclei were counterstained with DAPI (blue). Scale bar, 100 µm (n = 8/group). **(F and G)** Representative images of IHC staining of LOX (F) and quantification of LOX staining (G) in the breast tumors of MMTV-PyMT mice treated with vehicle or ProAgio. Scale bars, 100 µm (n = 6/group). **(H and I)** mRNA analysis of LOX (H), LOXL2 (left panel, I), and LOXL4 (right panel, I) measured by qRT-PCR in the tumors of 4T1 mice treated with vehicle (gray bar) or ProAgio (red bar). n = 4/group. **(J and K)** Quantification of LOX activity in the tumor extracts of 4T1 mice (J) and MMTV-PyMT mice (K) treated with vehicle or ProAgio (n = 5–6/group). **(L–O)** Representative images of Sirius red staining (left panels) and the corresponding cross-linked collagen images by polarized microscopy on Sirius red staining (right panels; L) and quantitative analysis of cross-linked collagen (M and N) in the breast tumors of 4T1 orthotopic (upper panels; n = 7/group) and MMTV-PyMT (lower panels; n = 5/group) mice treated with vehicle or ProAgio. Scale bars, 100 µm. **(O)** Quantification of cross-linked collagen per total collagen area in the breast tumor sections of 4T1 (left panel) and MMTV-PyMT mice (right panel) treated with vehicle (gray bar) or ProAgio (red bar); n = 4/group. Error bars in A, B, C, H, I, and K represent mean ± SEM. *, P < 0.05; **, P < 0.01; ***, P < 0.001; ****, P < 0.0001; ns denotes nonsignificant by unpaired Student's t test.

Sharma et al.
A novel treatment strategy for TNBC

Journal of Experimental Medicine   12 of 20
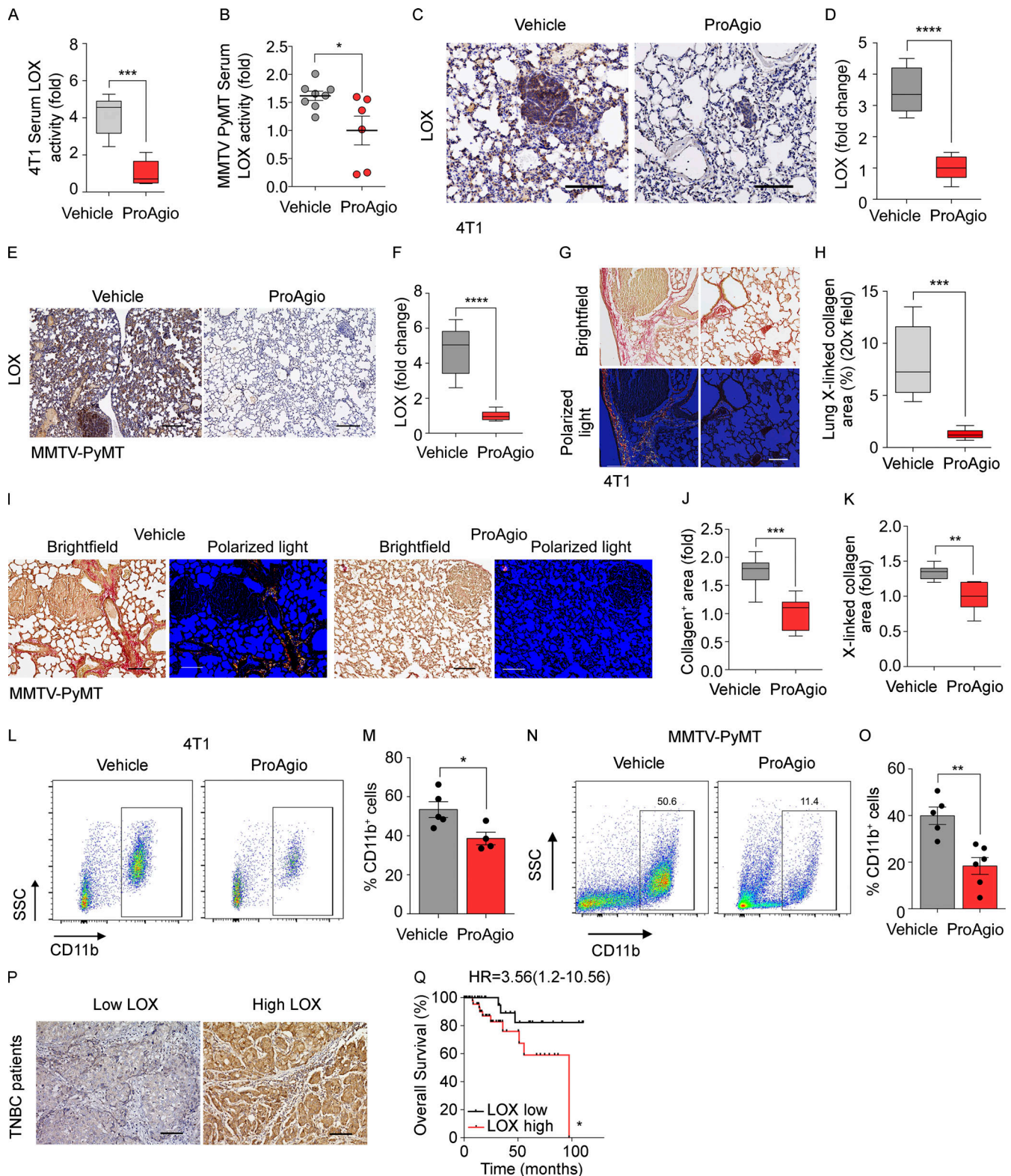https://doi.org/10.1084/jem.20200712

Figure 7. **ProAgio decreases hypoxia-induced LOX-mediated metastasis to the lungs in mouse models. (A and B)** Quantification of LOX activity in the serum of 4T1 orthotopic mice (n = 5–6/group; A) and MMTV-PyMT mice (n = 6–8/group; B) treated with vehicle or ProAgio. **(C–F)** Representative images of IHC staining of LOX (C and E) and quantification of LOX (D and F) in the lung metastatic tumors of 4T1 mice (C and D) and MMTV-PyMT mice (E and F) treated with vehicle or ProAgio (n = 6/group). Scale bars, 100 μm. **(G and H)** Representative images of Sirius red staining visualized under brightfield (upper panel) or polarized light microscopy (lower panel; G) and quantitative analysis of cross-linked collagen (under polarized light; H) in the lung metastatic tumors of 4T1 mice treated with vehicle or ProAgio. Scale bar, 100 μm (n = 7/group). **(I–K)** Representative images of Sirius red staining for collagen (left panel) and its corresponding cross-linked images by polarized microscopy on Sirius red staining (right panel; I) and quantification of collagen (J) and cross-linked collagen (K)

in the metastatic lungs of MMTV-PyMT mice treated with vehicle or ProAgio (n = 7/group). **(L–O)** Representative flow cytometric plots of CD11b (L and N) and the population of CD11b-positive cells (M and O) in the metastatic lungs of 4T1 mice (n = 4–5/group; M) and MMTV-PyMT mice (n = 5 or 6/group; O) treated with vehicle or ProAgio. SSC, side scatter. **(P)** Representative IHC images of low and high LOX staining in the breast tumors of TNBC patients (n = 80). Scale bars, 100 μm. **(Q)** Kaplan-Meier survival analysis of low and high LOX (low, n = 34; high, n = 48) gene expression in the breast tumors of TNBC patients. HR, hazard ratio. TCGA dataset of TNBC patients was obtained from cbioportal (https://www.cbioportal.org). Error bars in B, M, and O represent mean ± SEM. *, P < 0.05; **, P < 0.01; ***, P < 0.001; ****, P < 0.0001 by log-rank test (Q) or by unpaired Student's t test.

metastasis. Altogether, multiple effects of ProAgio due to depletion of CAFs and anti-angiogenesis (Fig. 9 F) enable the protein to be a promising treatment drug for TNBC, especially for patients with a tumor rich in dense fibrotic stroma.

Dense intratumoral collagen fibrils and leaky tumor vessels constitute barriers for drug delivery (Jain, 2005; Miao et al., 2015). Therefore, removal of dense collagen fibrils and reduction of leaky tumor angiogenic vasculature will enhance the delivery of chemotherapeutic agents. On the other hand, depletion of CAFs by ProAgio also decreases intratumoral levels of GFs that are mostly secreted by CAFs, which cuts off the crosstalk between cancer cells and CAFs. One important consequence is a reduction in cancer cell apoptosis resistance that is stimulated by intratumoral GFs. The dual action of ProAgio results in improved efficacy of the combination therapies (e.g., ProAgio + chemotherapy agents) in TNBC murine models. Importantly, the dual action of ProAgio allows achievement of a significant delay in tumor growth using a very low dose of chemotherapeutic agents (two- to sixfold less dosage of PTX and DOX). Significant lower dosage of cytotoxic anti-cancer drugs would greatly reduce the toxic side effects of the chemotherapeutic agents and improve treatment efficacy. The addition of checkpoint inhibitors to various chemotherapies represents an important advancement in the treatment of TNBC (D'Abreo and Adams, 2019; Vikas et al., 2018). It is well documented that CAFs play a critical role in modulating cancer immunity by secreting pro- or anti-inflammatory soluble factors, such as cytokines/chemokines (Barrett and Puré, 2020; Costa et al., 2018; Monteran and Erez, 2019). CAFs may also exclude cytotoxic T cells from cancer cells by inducing expression of immune-checkpoint and checkpoint ligands (Hanley and Thomas, 2020). In addition, CAFs may recruit myeloid cells to suppress tumor immunity (Costa et al., 2018; see Fig. 7, L–O).

Our study apparently introduces a strategy for TNBC treatment by simultaneously targeting stroma fibroblasts and angiogenic vessels by ProAgio, particularly in combination with other anti-cancer therapeutics. Due to important functions of CAFs in modulating cancer immunity, we anticipate that ProAgio in combination with immunotherapy may represent a promising potential treatment for TNBC patients.

Materials and methods
Cell lines, reagents, and PCR primers used in the study are listed in Table S1.

Primary fibroblasts and activation
hMFs and hLFs were purchased from Cell Biologics (H-6071) and Lonza (CC-2512), respectively, and cultured in complete fibroblast medium (Cell Biologics; M2267). The primary cells were activated by culturing in TGF-β (5 ng/ml) for 48 h. Human breast fibroblasts isolated from breast cancer patients (hbCAFs) were purchased from Neuromics (CAF06) and cultured in MSC-GRO low serum, complete medium (SC00B1).

Cell hypoxia
MDA-MB-231 or 4T1 cells were cultured in a modular incubator chamber that was infused with a mixture of 1% O_2, 5% CO_2, and 94% N_2 at 37°C for the indicated time.

Mouse CAF isolation from 4T1 tumor (procedure adopted from F. Calvo and coworkers [Calvo et al., 2013])
Tumor from a 4T1 mouse (around 500–700 mm³) was minced into small pieces and digested by collagenase. After filtering the undigested tissue, the solution was serial centrifuged, and the final pellet was resuspended in DMEM with 10% FBS and 1% insulin–transferrin–selenium (Thermo Fisher Scientific; #41400-045) and seeded on a culture dish. After 30 min, the fibroblasts had already adhered to the dish, whereas other cell types remained in suspension. Fibroblasts were subsequently grown on a culture dish, and the population was expanded.

MMTV-PyMT, orthotopic MDA-MB-231, and 4T1 mice generation and treatments and patient tissue sample screening
All animal experiments were performed under the approval of the Institutional Animal Care and Use Committee of Georgia State University. For the MDA-MB-231 xenograft, MDA-MB-231 cells (5 × 10⁶) were implanted into the mammary gland of female nude mice. Tumor growth was measured using a caliper ruler. For MMTV-PyMT (FVB/N genetic background), hemizygous male MMTV-PyMT and noncarrier female mice were purchased from The Jackson Laboratory (Stock no. 002374, strain name: Tg(MMTV-PyVT)634Mul). A colony was established and maintained in our animal facility by crossing MMTV-PyMT male mice to wild-type female mice on FVB/N background. The offspring were genotyped by PCR using primers listed in Table S1. Female mice positive for MMTV-PyMT were used in the study. Nontransgenic littermate females (MMTV-PyMT negative) were used as controls. For 4T1 orthotopic, 4T1 cells (5 × 10⁵) were implanted into the mammary gland of female Balb/C mice. Tumor growth was measured using a caliper ruler. For the 4T1 spontaneous model, 4T1 cells (1 × 10⁴) were injected i.v. into the tail vein of female Balb/C mice. For MDA-MB-231 mice, treatments were started when tumors grew to an average size of 150 mm³. For 4T1 mice, treatments were started when tumors grew to an average size of 250 mm³. For the 4T1 spontaneous model, treatments were started the next day after cancer cell injection. For MMTV-PyMT mice, treatments were started at
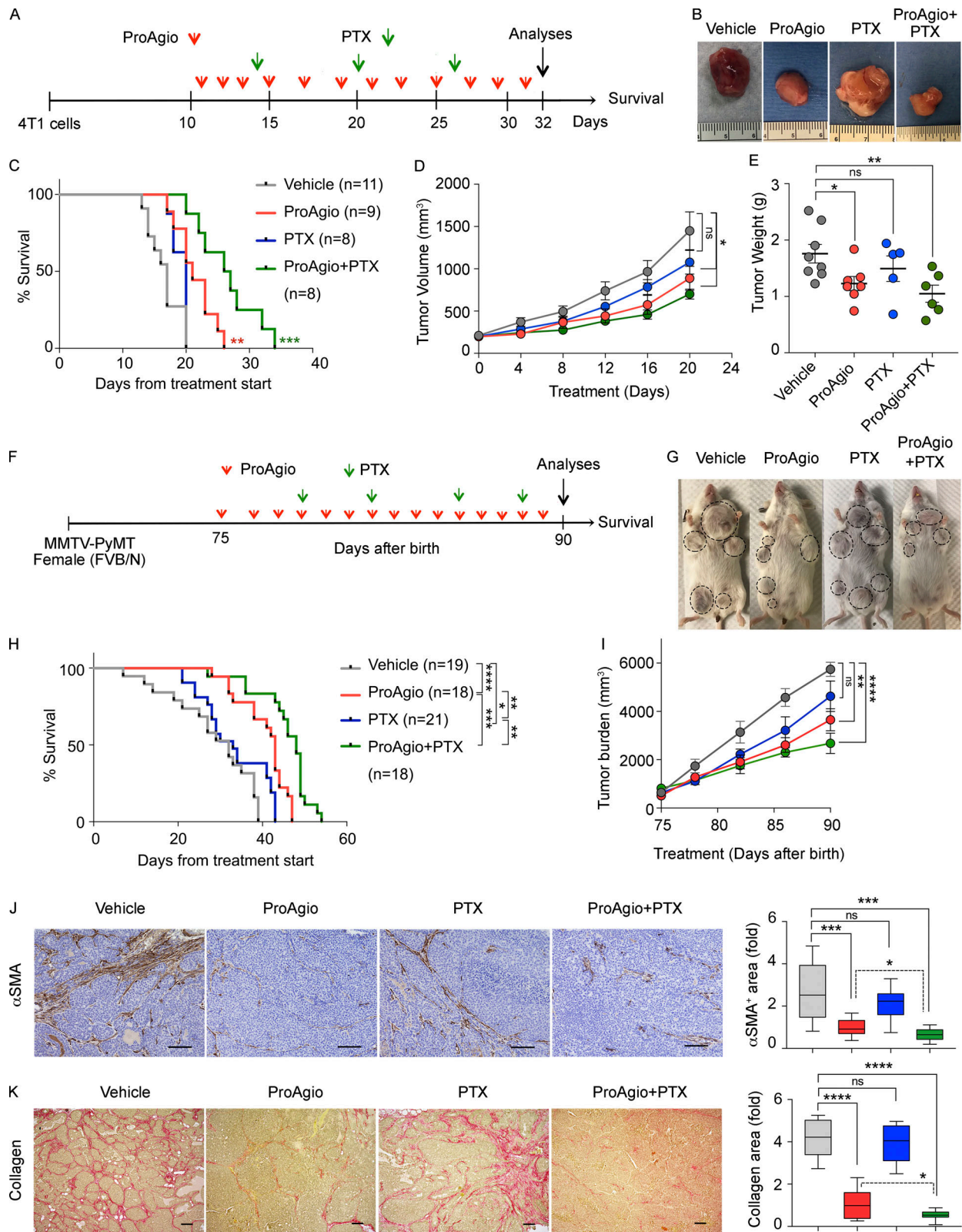
Figure 8. **ProAgio enhances chemotherapeutic efficacy in 4T1 orthotopic and MMTV-PyMT mouse models. (A)** Therapy regimen of ProAgio (red arrows) and PTX (green arrows, i.p. 3 mg/kg) in 4T1 mice. **(B)** Representative images of tumors of 4T1 mice treated with indicated agents. **(C–E)** Kaplan-Meier survival plot (n = 8–11; median survival [days]: vehicle = 17, ProAgio = 21, PTX = 20, ProAgio + PTX = 26.5; C), mean tumor volume (n = 8–12; D), and mean tumor weight (E) of 4T1 mice treated with indicated agents (n = 5–8). **(F)** Therapy regimen of ProAgio (red arrows) and PTX (green arrows, i.p. 5 mg/kg) in MMTV-PyMT mice. **(G)** Representative images showing appearance of tumors indicated by dotted circles on MMTV-PyMT mice treated with indicated agents. **(H and I)** Kaplan-Meier survival analysis (n = 18–21; median survival [days]: vehicle = 32, ProAgio = 43, PTX = 33, ProAgio + PTX = 48; H), mean tumor burden

(total volumes of all tumors; I) of MMTV-PyMT mice treated with indicated agents (*n* = 6–8). **(J and K)** Representative images of IHC staining and quantitative analyses of α-SMA (J) and Sirius red staining and quantitative analyses of collagen (K) in the breast tumors of MMTV-PyMT mice treated with indicated agents**.** Scale bars, 100 µm (*n* = 4–6/group). Error bars in D, E and I represent mean ± SEM. *, P < 0.05; **, P < 0.01; ***, P < 0.001; ****; P < 0.0001; ns denotes nonsignificant by log-rank test (C and H) or unpaired Student's *t* test.

---

75 d of age. Mice were randomly enrolled in treatment groups. At the end of the treatments, animals were either sacrificed for analyses or maintained in the cages for survival assessment. Organs, tumor tissues, and blood samples were collected at the end of the experiments for subsequent analyses. Treatment schedule and dosages are specified in the figures or legends. Statistical analyses were done in comparison to the control group.

Patient tissue analyses were performed under the guidelines of the National Institutes of Health. All tissue samples are de-identified. It falls under Institutional Review Board exemption 4. Samples were sectioned and analyzed by different staining. Samples were obtained from either US Biomax or Harbin Medical University Cancer Hospital, China (*n* = 80). Studies were performed under the approval of the Institutional Review Board of Georgia State University and Harbin Medical University.

Analysis of publicly available datasets
The gene expression profile of TNBC patients was analyzed by obtaining data from The Cancer Genom Atlas (TCGA), Cell 2015, by using https://www.cbioportal.org.

Tissue section staining and quantitation
Sirius red staining was performed using kits obtained from IHC World by following the vendor's instructions.

IHC and IF
IHC and IF staining procedures were similar to those of previous reports (Turaga et al., 2016). Images were captured at various magnifications indicated by scale bars.

Quantitation of Sirius red, IHC, and IF staining was performed using ImageJ. Quantifications are positive stain areas in each view field or fold change by comparing to the controls unless otherwise specified in the figures and legends. All quantitation results were means of randomly selected three view fields per section, five sections per animal, and 6–10 mice per experimental group unless otherwise specified in the figures and legends.

LOX activity assay (adopted from Fogelgren et al., 2005)
Blood or tumor tissues were taken from experimental animals at the end of the experiments. Serum and tumor lysates were prepared. LOX activity was measured using a LOX activity kit.

Tumor hypoxia
Hypoxyprobe-1 (60 mg/kg, solid pimonidazole hydrochloride) was i.v. injected in the mice 1 h before extraction. Sections were prepared from the harvested tumors. The sections were IHC stained per the vendor's instructions.

PTX concentration by HPLC
PTX stock solution was prepared at 500 µg/ml, and 10, 25, 50, 75, and 100 µg/ml was prepared by dilution of the stock in

methanol. The Agilent UHPLC system with an Agilent C_{18} column was used. The mobile phase was acetonitrile (ACN)/sodium acetate buffer (0.01 M, pH 5.0) at 60/40 with a flow rate of 1 ml/min. 1 g of tumor was weighed and ground in liquid nitrogen. The samples were subjected to extraction with diethyl-ether. Samples were centrifuged at 14,000 rpm for 10 min. The organic layer was separated. 50 µl of the sample was then injected into the system for analysis.

Vascular leakage and perfusion assays (adopted from Park et al., 2016)
At the end of the 4T1 experiment, tumor vessel leakage was analyzed after i.v. injection of 100 µl of FITC-conjugated dextran (25 mg/ml) 30 min before sacrifice. For vascular perfusion studies, 100 µl of 594-conjugated tomato lectin (1 mg/ml) was i.v. injected 30 min before sacrifice.

Cell sorting using MACS cell separation kit (adopted from Wong et al., 1995)
The breast tumor tissue sample (∼100 mg) was cut, minced, and then dissociated in a solution comprising RPMI media and collagenase in gentleMACS dissociator (Miltenyi Biotec). It was followed by RBC lysis using Red Blood Cell Lysis Solution (Miltenyi Biotec; Catalog #130-094-183). Dead cells were removed by centrifugation, and cell suspension was subsequently pelleted. mRNA was isolated from the tumor cells. Next, the pellet was resuspended and labeled with anti-CD31 (Catalog #14–0319-82) mouse IgG antibody followed by magnetic separation. mRNA was isolated from the magnetically labeled cells, and RT-PCR was performed for integrin $α_V$ and integrin $β_3$. β-actin was used as a loading control. Further, flow through containing unlabeled cells was used to isolate CAFs using anti-PDGFRβ mouse IgG antibody (Catalog #MA5-15103), and mRNA was subsequently isolated. The remaining flow was also collected to isolate mRNA.

The procedures for angiogenesis analysis, qRT-PCR, immunoprecipitation, Western blotting, apoptosis assay, MTT (3-(4,5-dimethylthiazol-2-yl)-2,5-diphenyl tetrazolium bromide) assay, and flow cytometry were adopted from our previous reports (Li et al., 2014; Turaga et al., 2016; Zhang et al., 2016).

Statistical calculations
Statistical analyses were performed using GraphPad Prism 6.0 software. Kaplan-Meier survival curves were calculated using survival time for each mouse from all treatment groups. Statistical analyses in the survival experiments were performed by log-rank (Mantel-Cox) test. All in vitro experiments were performed at least three or four times. For tumor burden analyses, image quantifications, and other analyses, statistical significance was assayed by unpaired Student's *t* test. Box plots show range, median, and quartiles. In all figures, *, P < 0.05; **, P < 0.01; ***,
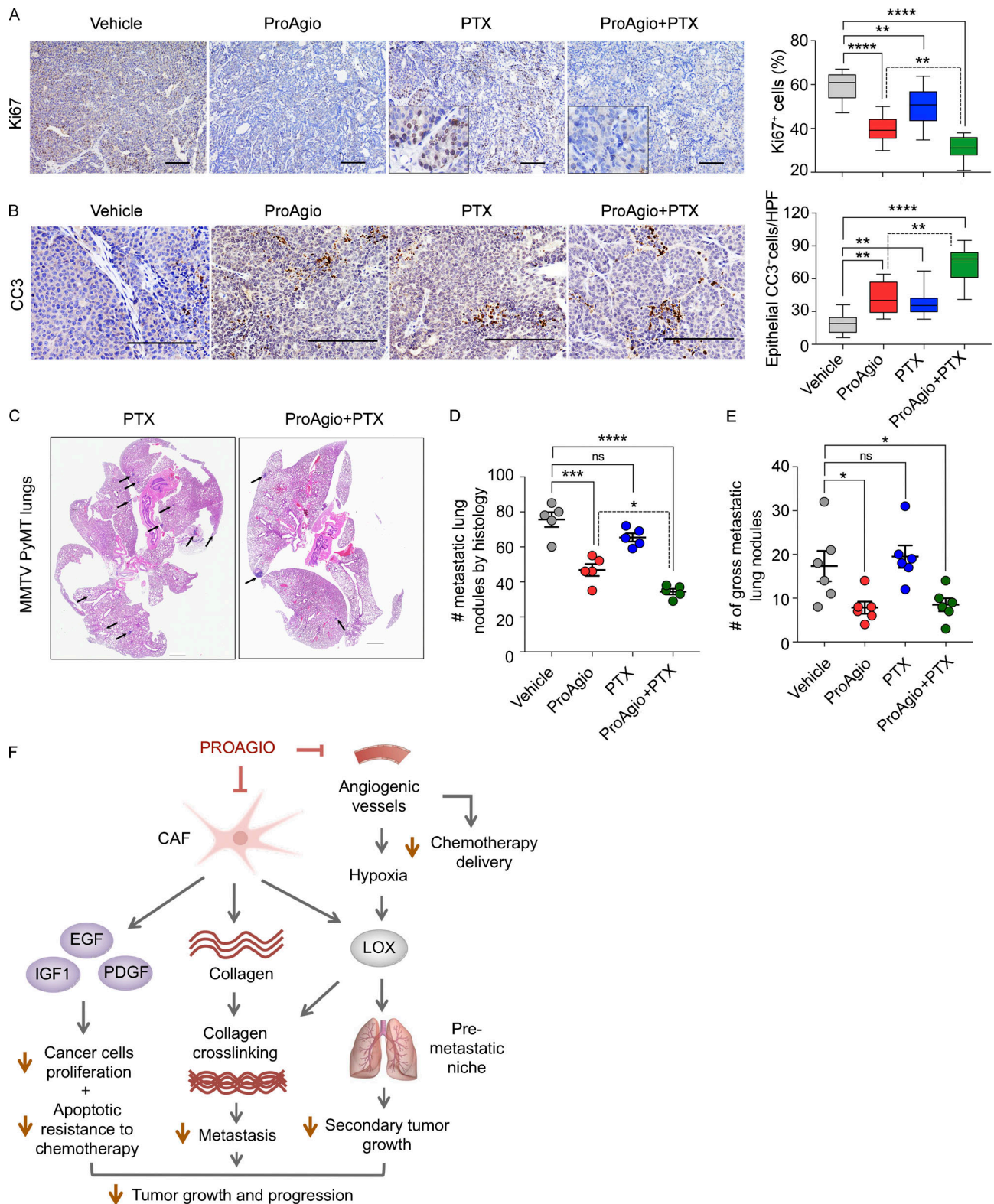
Figure 9. **ProAgio enhances the efficacy of chemotherapeutics. (A and B)** Representative images of IHC staining and quantitative analyses of Ki67 (A) and CC3 (B) in the breast tumors of MMTV-PyMT mice treated with indicated agents. Insets, ×3; Scale bars, 100 μm (n = 4–6/group). **(C–E)** Representative H&E images of lung sections (C), number of metastatic lung nodules by histology (D), and number of metastatic lung nodules on the lung surface (E) of MMTV-PyMT mice treated with indicated agents. Black arrows indicate metastatic nodules in lungs. Scale bars, 1,000 μm (n = 5–6/group). **(F)** Schematic illustration of action of ProAgio in TNBC. Error bars in D and E represent mean ± SEM. *, $P < 0.05$; **, $P < 0.01$; ***, $P < 0.001$; ****, $P < 0.001$; ns denotes nonsignificant by unpaired Student's t test.

P < 0.001; and ****, P < 0.0001; ns denotes not significant. All data are presented as mean ± SEM or as box plots.

Online supplemental material

Fig. S1 shows that high stroma is associated with poor overall survival and disease-free survival (DFS); breast cancer CAFs express high levels of integrin $\alpha_v\beta_3$; there is a close correlation between integrin β_3, α-SMA, and FAP levels in TNBC patient tissue samples; and ProAgio induces apoptosis in breast cancer CAFs. Fig. S2 shows that ProAgio does not induce apoptosis in TNBC cell lines because they do not express integrin $\alpha_v\beta_3$; ProAgio decreases cancer cell proliferation in mouse models; and ProAgio reduces levels of α-SMA by inducing apoptosis in breast cancer CAFs and mediates apoptosis in cancer cells, although apoptosis in breast cancer CAFs is much higher than cancer cells. Fig. S3 shows that ProAgio reduces levels of GFs and signaling downstream; the addition of GFs or CAF-conditioned media mediates apoptotic resistance in cancer cells; and ProAgio induces apoptosis in breast CAFs and therefore sensitizes cancer cells to apoptotic induction by a chemotherapeutic agent. Fig. S4 illustrates that ProAgio treatment reduces the number and size of metastatic lung nodules in mouse models and ProAgio treatment induces apoptosis in integrin $\alpha_v\beta_3$-expressing activated lung fibroblasts and decreases α-SMA and collagen levels in metastatic lungs in mouse models. Fig. S5 elucidates that ProAgio enhances the effect of chemotherapeutics in mouse models. Table S1 lists all cell lines, reagents, antibodies, PCR primers, and kits used in the study.

References

Antonyak, M.A., A.M. Miller, J.M. Jansen, J.E. Boehm, C.E. Balkman, J.J. Wakshlag, R.L. Page, and R.A. Cerione. 2004. Augmentation of tissue transglutaminase expression and activation by epidermal growth factor inhibit doxorubicin-induced apoptosis in human breast cancer cells. *J. Biol. Chem.* 279:41461–41467. https://doi.org/10.1074/jbc.M404976200

Attieh, Y., A.G. Clark, C. Grass, S. Richon, M. Pocard, P. Mariani, N. Elkhatib, T. Betz, B. Gurchenkov, and D.M. Vignjevic. 2017. Cancer-associated fibroblasts lead tumor invasion through integrin-β3-dependent fibronectin assembly. *J. Cell Biol.* 216:3509–3520. https://doi.org/10.1083/jcb.201702033

Barnett, R.M., and E. Vilar. 2018. Targeted Therapy for Cancer-Associated Fibroblasts: Are We There Yet? *J. Natl. Cancer Inst.* 110:11–13. https://doi.org/10.1093/jnci/djx131

Barrett, R., and E. Puré. 2020. Cancer-associated fibroblasts: key determinants of tumor immunity and immunotherapy. *Curr. Opin. Immunol.* 64:80–87. https://doi.org/10.1016/j.coi.2020.03.004

Baumgartner, G., C. Gomar-Höss, L. Sakr, E. Ulsperger, and C. Wogritsch. 1998. The impact of extracellular matrix on the chemoresistance of solid tumors--experimental and clinical results of hyaluronidase as additive to cytostatic chemotherapy. *Cancer Lett.* 131:85–99. https://doi.org/10.1016/S0304-3835(98)00204-3

Brooks, P.C., R.A. Clark, and D.A. Cheresh. 1994. Requirement of vascular integrin alpha v beta 3 for angiogenesis. *Science.* 264:569–571. https://doi.org/10.1126/science.7512751

Calvo, F., N. Ege, A. Grande-Garcia, S. Hooper, R.P. Jenkins, S.I. Chaudhry, K. Harrington, P. Williamson, E. Moeendarbary, G. Charras, and E. Sahai. 2013. Mechanotransduction and YAP-dependent matrix remodelling is required for the generation and maintenance of cancer-associated fibroblasts. *Nat. Cell Biol.* 15:637–646. https://doi.org/10.1038/ncb2756

Carmeliet, P., and R.K. Jain. 2000. Angiogenesis in cancer and other diseases. *Nature.* 407:249–257. https://doi.org/10.1038/35025220

Chen, X., and E. Song. 2019. Turning foes to friends: targeting cancer-associated fibroblasts. *Nat. Rev. Drug Discov.* 18:99–115. https://doi.org/10.1038/s41573-018-0004-1

Christenson, J.L., K.T. Butterfield, N.S. Spoelstra, J.D. Norris, J.S. Josan, J.A. Pollock, D.P. McDonnell, B.S. Katzenellenbogen, J.A. Katzenellenbogen, and J.K. Richer. 2017. MMTV-PyMT and Derived Met-1 Mouse Mammary Tumor Cells as Models for Studying the Role of the Androgen Receptor in Triple-Negative Breast Cancer Progression. *Horm. Cancer.* 8:69–77. https://doi.org/10.1007/s12672-017-0285-6

Cleator, S., W. Heller, and R.C. Coombes. 2007. Triple-negative breast cancer: therapeutic options. *Lancet Oncol.* 8:235–244. https://doi.org/10.1016/S1470-2045(07)70074-8

Costa, A., Y. Kieffer, A. Scholer-Dahirel, F. Pelon, B. Bourachot, M. Cardon, P. Sirven, I. Magagna, L. Fuhrmann, C. Bernard, et al. 2018. Fibroblast Heterogeneity and Immunosuppressive Environment in Human Breast Cancer. *Cancer Cell.* 33:463–479.e10. https://doi.org/10.1016/j.ccell.2018.01.011

D'Abreo, N., and S. Adams. 2019. Immune-checkpoint inhibition for metastatic triple-negative breast cancer: safety first? *Nat. Rev. Clin. Oncol.* 16:399–400. https://doi.org/10.1038/s41571-019-0216-2

de Kruijf, E.M., J.G. van Nes, C.J. van de Velde, H. Putter, V.T. Smit, G.J. Liefers, P.J. Kuppen, R.A. Tollenaar, and W.E. Mesker. 2011. Tumor-stroma ratio in the primary tumor is a prognostic factor in early breast cancer patients, especially in triple-negative carcinoma patients. *Breast Cancer Res. Treat.* 125:687–696. https://doi.org/10.1007/s10549-010-0855-6

Dias, A.S., C.R. Almeida, L.A. Helguero, and I.F. Duarte. 2019. Metabolic crosstalk in the breast cancer microenvironment. *Eur. J. Cancer.* 121:154–171. https://doi.org/10.1016/j.ejca.2019.09.002

Emon, B., J. Bauer, Y. Jain, B. Jung, and T. Saif. 2018. Biophysics of Tumor Microenvironment and Cancer Metastasis - A Mini Review. *Comput. Struct. Biotechnol. J.* 16:279–287. https://doi.org/10.1016/j.csbj.2018.07.003

Fingas, C.D., S.F. Bronk, N.W. Werneburg, J.L. Mott, M.E. Guicciardi, S.C. Cazanave, J.C. Mertens, A.E. Sirica, and G.J. Gores. 2011. Myofibroblast-derived PDGF-BB promotes Hedgehog survival signaling in cholangiocarcinoma cells. *Hepatology.* 54:2076–2088. https://doi.org/10.1002/hep.24588

Fogelgren, B., N. Polgár, K.M. Szauter, Z. Ujfaludi, R. Laczkó, K.S. Fong, and K. Csiszar. 2005. Cellular fibronectin binds to lysyl oxidase with high affinity and is critical for its proteolytic activation. *J. Biol. Chem.* 280:24690–24697. https://doi.org/10.1074/jbc.M412979200

Foulkes, W.D., I.E. Smith, and J.S. Reis-Filho. 2010. Triple-negative breast cancer. *N. Engl. J. Med.* 363:1938–1948. https://doi.org/10.1056/NEJMra1001389

Fox, S.B., D.G. Generali, and A.L. Harris. 2007. Breast tumour angiogenesis. *Breast Cancer Res.* 9:216. https://doi.org/10.1186/bcr1796

Fushida-Takemura, H., M. Fukuda, N. Maekawa, M. Chanoki, H. Kobayashi, N. Yashiro, M. Ishii, T. Hamada, S. Otani, and A. Ooshima. 1996. Detection of lysyl oxidase gene expression in rat skin during wound healing. *Arch. Dermatol. Res.* 288:7–10. https://doi.org/10.1007/BF02505035

Haffty, B.G., Q. Yang, M. Reiss, T. Kearney, S.A. Higgins, J. Weidhaas, L. Harris, W. Hait, and D. Toppmeyer. 2006. Locoregional relapse and distant metastasis in conservatively managed triple negative early-stage breast cancer. *J. Clin. Oncol.* 24:5652–5657. https://doi.org/10.1200/JCO.2006.06.5664

Hanley, C.J., and G.J. Thomas. 2020. T-cell tumour exclusion and immunotherapy resistance: a role for CAF targeting. *Br. J. Cancer.* 123:1353–1355. https://doi.org/10.1038/s41416-020-1020-6

Havaki, S., M. Kouloukoussa, K. Amawi, Y. Drosos, L.D. Arvanitis, N. Goutas, D. Vlachodimitropoulos, S.D. Vassilaros, E.Z. Katsantoni, I. Voloudakis-Baltatzis, et al. 2007. Altered expression pattern of integrin alphavbeta3 correlates with actin cytoskeleton in primary cultures of human breast cancer. *Cancer Cell Int.* 7:16. https://doi.org/10.1186/1475-2867-7-16

Huelsken, J., and D. Hanahan. 2018. A Subset of Cancer-Associated Fibroblasts Determines Therapy Resistance. *Cell.* 172:643–644. https://doi.org/10.1016/j.cell.2018.01.028

Jain, R.K. 2005. Normalization of tumor vasculature: an emerging concept in antiangiogenic therapy. *Science.* 307:58–62. https://doi.org/10.1126/science.1104819

Ji, F., Y. Wang, L. Qiu, S. Li, J. Zhu, Z. Liang, Y. Wan, and W. Di. 2013. Hypoxia inducible factor 1α-mediated LOX expression correlates with migration and invasion in epithelial ovarian cancer. *Int. J. Oncol.* 42:1578–1588. https://doi.org/10.3892/ijo.2013.1878

Jonkers, J., and P.W. Derksen. 2007. Modeling metastatic breast cancer in mice. *J. Mammary Gland Biol. Neoplasia.* 12:191–203. https://doi.org/10.1007/s10911-007-9050-8

Kalluri, R. 2016. The biology and function of fibroblasts in cancer. *Nat. Rev. Cancer.* 16:582–598. https://doi.org/10.1038/nrc.2016.73

Kugeratski, F.G., S.J. Atkinson, L.J. Neilson, S. Lilla, J.R.P. Knight, J. Serneels, A. Juin, S. Ismail, D.M. Bryant, E.K. Markert, et al. 2019. Hypoxic cancer-associated fibroblasts increase NCBP2-AS2/HIAR to promote endothelial sprouting through enhanced VEGF signaling. *Sci. Signal.* 12: eaan8247. https://doi.org/10.1126/scisignal.aan8247

LeBleu, V.S., and R. Kalluri. 2018. A peek into cancer-associated fibroblasts: origins, functions and translational impact. *Dis. Model. Mech.* 11: dmm029447. https://doi.org/10.1242/dmm.029447

Li, L., Y. Zhang, J. Qiao, J.J. Yang, and Z.R. Liu. 2014. Pyruvate kinase M2 in blood circulation facilitates tumor growth by promoting angiogenesis. *J. Biol. Chem.* 289:25812–25821. https://doi.org/10.1074/jbc.M114.576934

Liapis, H., A. Flath, and S. Kitazawa. 1996. Integrin alpha V beta 3 expression by bone-residing breast cancer metastases. *Diagn. Mol. Pathol.* 5:127–135. https://doi.org/10.1097/00019606-199606000-00008

Linderholm, B.K., H. Hellborg, U. Johansson, G. Elmberger, L. Skoog, J. Lehtiö, and R. Lewensohn. 2009. Significantly higher levels of vascular endothelial growth factor (VEGF) and shorter survival times for patients with primary operable triple-negative breast cancer. *Ann. Oncol.* 20: 1639–1646. https://doi.org/10.1093/annonc/mdp062

Lopes-Bastos, B.M., W.G. Jiang, and J. Cai. 2016. Tumour-Endothelial Cell Communications: Important and Indispensable Mediators of Tumour Angiogenesis. *Anticancer Res.* 36:1119–1126.

Mayrand, D., A. Laforce-Lavoie, S. Larochelle, A. Langlois, H. Genest, M. Roy, and V.J. Moulin. 2012. Angiogenic properties of myofibroblasts isolated from normal human skin wounds. *Angiogenesis.* 15:199–212. https://doi.org/10.1007/s10456-012-9253-5

Miao, L., C.M. Lin, and L. Huang. 2015. Stromal barriers and strategies for the delivery of nanomedicine to desmoplastic tumors. *J. Control. Release.* 219:192–204. https://doi.org/10.1016/j.jconrel.2015.08.017

Mohammed, R.A., I.O. Ellis, A.M. Mahmmod, E.C. Hawkes, A.R. Green, E.A. Rakha, and S.G. Martin. 2011. Lymphatic and blood vessels in basal and triple-negative breast cancers: characteristics and prognostic significance. *Mod. Pathol.* 24:774–785. https://doi.org/10.1038/modpathol.2011.4

Monteran, L., and N. Erez. 2019. The Dark Side of Fibroblasts: Cancer-Associated Fibroblasts as Mediators of Immunosuppression in the Tumor Microenvironment. *Front. Immunol.* 10:1835. https://doi.org/10.3389/fimmu.2019.01835

Moorman, A.M., R. Vink, H.J. Heijmans, J. van der Palen, and E.A. Kouwenhoven. 2012. The prognostic value of tumour-stroma ratio in triple-negative breast cancer. *Eur. J. Surg. Oncol.* 38:307–313. https://doi.org/10.1016/j.ejso.2012.01.002

Neve, A., F.P. Cantatore, N. Maruotti, A. Corrado, and D. Ribatti. 2014. Extracellular matrix modulates angiogenesis in physiological and pathological conditions. *BioMed Res. Int.* 2014:756078. https://doi.org/10.1155/2014/756078

O'Shaughnessy, J., C. Osborne, J.E. Pippen, M. Yoffe, D. Patt, C. Rocha, I.C. Koo, B.M. Sherman, and C. Bradley. 2011. Iniparib plus chemotherapy in metastatic triple-negative breast cancer. *N. Engl. J. Med.* 364:205–214. https://doi.org/10.1056/NEJMoa1011418

Öhlund, D., E. Elyada, and D. Tuveson. 2014. Fibroblast heterogeneity in the cancer wound. *J. Exp. Med.* 211:1503–1523. https://doi.org/10.1084/jem.20140692

Öhlund, D., A. Handly-Santana, G. Biffi, E. Elyada, A.S. Almeida, M. Ponz-Sarvise, V. Corbo, T.E. Oni, S.A. Hearn, E.J. Lee, et al. 2017. Distinct populations of inflammatory fibroblasts and myofibroblasts in pancreatic cancer. *J. Exp. Med.* 214:579–596. https://doi.org/10.1084/jem.20162024

Park, J.S., I.K. Kim, S. Han, I. Park, C. Kim, J. Bae, S.J. Oh, S. Lee, J.H. Kim, D.C. Woo, et al. 2016. Normalization of Tumor Vessels by Tie2 Activation and Ang2 Inhibition Enhances Drug Delivery and Produces a Favorable Tumor Microenvironment. *Cancer Cell.* 30:953–967. https://doi.org/10.1016/j.ccell.2016.10.018

Pickup, M.W., H. Laklai, I. Acerbi, P. Owens, A.E. Gorska, A. Chytil, M. Aakre, V.M. Weaver, and H.L. Moses. 2013. Stromally derived lysyl oxidase promotes metastasis of transforming growth factor-β-deficient mouse mammary carcinomas. *Cancer Res.* 73:5336–5346. https://doi.org/10.1158/0008-5472.CAN-13-0012

Polydorou, C., F. Mpekris, P. Papageorgis, C. Voutouri, and T. Stylianopoulos. 2017. Pirfenidone normalizes the tumor microenvironment to improve chemotherapy. *Oncotarget.* 8:24506–24517. https://doi.org/10.18632/oncotarget.15534

Quail, D.F., and J.A. Joyce. 2013. Microenvironmental regulation of tumor progression and metastasis. *Nat. Med.* 19:1423–1437. https://doi.org/10.1038/nm.3394

Rachman-Tzemah, C., S. Zaffryar-Eilot, M. Grossman, D. Ribero, M. Timaner, J.M. Mäki, J. Myllyharju, F. Bertolini, D. Hershkovitz, I. Sagi, et al. 2017. Blocking Surgically Induced Lysyl Oxidase Activity Reduces the Risk of Lung Metastases. *Cell Rep.* 19:774–784.

Rankin, E.B., and A.J. Giaccia. 2016. Hypoxic control of metastasis. *Science.* 352:175–180. https://doi.org/10.1126/science.aaf4405

Relf, M., S. LeJeune, P.A. Scott, S. Fox, K. Smith, R. Leek, A. Moghaddam, R. Whitehouse, R. Bicknell, and A.L. Harris. 1997. Expression of the angiogenic factors vascular endothelial cell growth factor, acidic and basic fibroblast growth factor, tumor growth factor beta-1, platelet-derived endothelial cell growth factor, placenta growth factor, and pleiotrophin in human primary breast cancer and its relation to angiogenesis. *Cancer Res.* 57:963–969.

Ribatti, D., B. Nico, S. Ruggieri, R. Tamma, G. Simone, and A. Mangia. 2016. Angiogenesis and Antiangiogenesis in Triple-Negative Breast cancer. *Transl. Oncol.* 9:453–457. https://doi.org/10.1016/j.tranon.2016.07.002

Sahai, E., I. Astsaturov, E. Cukierman, D.G. DeNardo, M. Egeblad, R.M. Evans, D. Fearon, F.R. Greten, S.R. Hingorani, T. Hunter, et al. 2020. A framework for advancing our understanding of cancer-associated fibroblasts. *Nat. Rev. Cancer.* 20:174–186. https://doi.org/10.1038/s41568-019-0238-1

Sewell-Loftin, M.K., S.V.H. Bayer, E. Crist, T. Hughes, S.M. Joison, G.D. Longmore, and S.C. George. 2017. Cancer-associated fibroblasts support

vascular growth through mechanical force. *Sci. Rep.* 7:12574. https://doi.org/10.1038/s41598-017-13006-x

Su, S., J. Chen, H. Yao, J. Liu, S. Yu, L. Lao, M. Wang, M. Luo, Y. Xing, F. Chen, et al. 2018. CD10+GPR77+ Cancer-Associated Fibroblasts Promote Cancer Formation and Chemoresistance by Sustaining Cancer Stemness. *Cell.* 172:841–856.e16. https://doi.org/10.1016/j.cell.2018.01.009

Takai, K., A. Le, V.M. Weaver, and Z. Werb. 2016. Targeting the cancer-associated fibroblasts as a treatment in triple-negative breast cancer. *Oncotarget.* 7:82889–82901. https://doi.org/10.18632/oncotarget.12658

Turaga, R.C., L. Yin, J.J. Yang, H. Lee, I. Ivanov, C. Yan, H. Yang, H.E. Grossniklaus, S. Wang, C. Ma, et al. 2016. Rational design of a protein that binds integrin αvβ3 outside the ligand binding site. *Nat. Commun.* 7:11675. https://doi.org/10.1038/ncomms11675

Vikas, P., N. Borcherding, and W. Zhang. 2018. The clinical promise of immunotherapy in triple-negative breast cancer. *Cancer Manag. Res.* 10:6823–6833. https://doi.org/10.2147/CMAR.S185176

Vong, S., and R. Kalluri. 2011. The role of stromal myofibroblast and extracellular matrix in tumor angiogenesis. *Genes Cancer.* 2:1139–1145. https://doi.org/10.1177/1947601911423940

Wang, F.T., W. Sun, J.T. Zhang, and Y.Z. Fan. 2019. Cancer-associated fibroblast regulation of tumor neo-angiogenesis as a therapeutic target in cancer. *Oncol. Lett.* 17:3055–3065. https://doi.org/10.3892/ol.2019.9973

Wong, L.S., W.J. Bateman, A.G. Morris, and I.A. Fraser. 1995. Detection of circulating tumour cells with the magnetic activated cell sorter. *Br. J. Surg.* 82:1333–1337. https://doi.org/10.1002/bjs.1800821012

Wong, C.C., D.M. Gilkes, H. Zhang, J. Chen, H. Wei, P. Chaturvedi, S.I. Fraley, C.M. Wong, U.S. Khoo, I.O. Ng, et al. 2011. Hypoxia-inducible factor 1 is a master regulator of breast cancer metastatic niche formation. *Proc. Natl. Acad. Sci. USA.* 108:16369–16374. https://doi.org/10.1073/pnas.1113483108

Wong, C.C., H. Zhang, D.M. Gilkes, J. Chen, H. Wei, P. Chaturvedi, M.E. Hubbi, and G.L. Semenza. 2012. Inhibitors of hypoxia-inducible factor 1 block breast cancer metastatic niche formation and lung metastasis. *J. Mol. Med. (Berl.).* 90:803–815. https://doi.org/10.1007/s00109-011-0855-y

Zhang, K., C.A. Corsa, S.M. Ponik, J.L. Prior, D. Piwnica-Worms, K.W. Eliceiri, P.J. Keely, and G.D. Longmore. 2013. The collagen receptor discoidin domain receptor 2 stabilizes SNAIL1 to facilitate breast cancer metastasis. *Nat. Cell Biol.* 15:677–687. https://doi.org/10.1038/ncb2743

Zhang, Y., L. Li, Y. Liu, and Z.R. Liu. 2016. PKM2 released by neutrophils at wound site facilitates early wound healing by promoting angiogenesis. *Wound Repair Regen.* 24:328–336. https://doi.org/10.1111/wrr.12411

Zhou, X., R.G. Rowe, N. Hiraoka, J.P. George, D. Wirtz, D.F. Mosher, I. Virtanen, M.A. Chernousov, and S.J. Weiss. 2008. Fibronectin fibrillogenesis regulates three-dimensional neovessel formation. *Genes Dev.* 22:1231–1243. https://doi.org/10.1101/gad.1643308
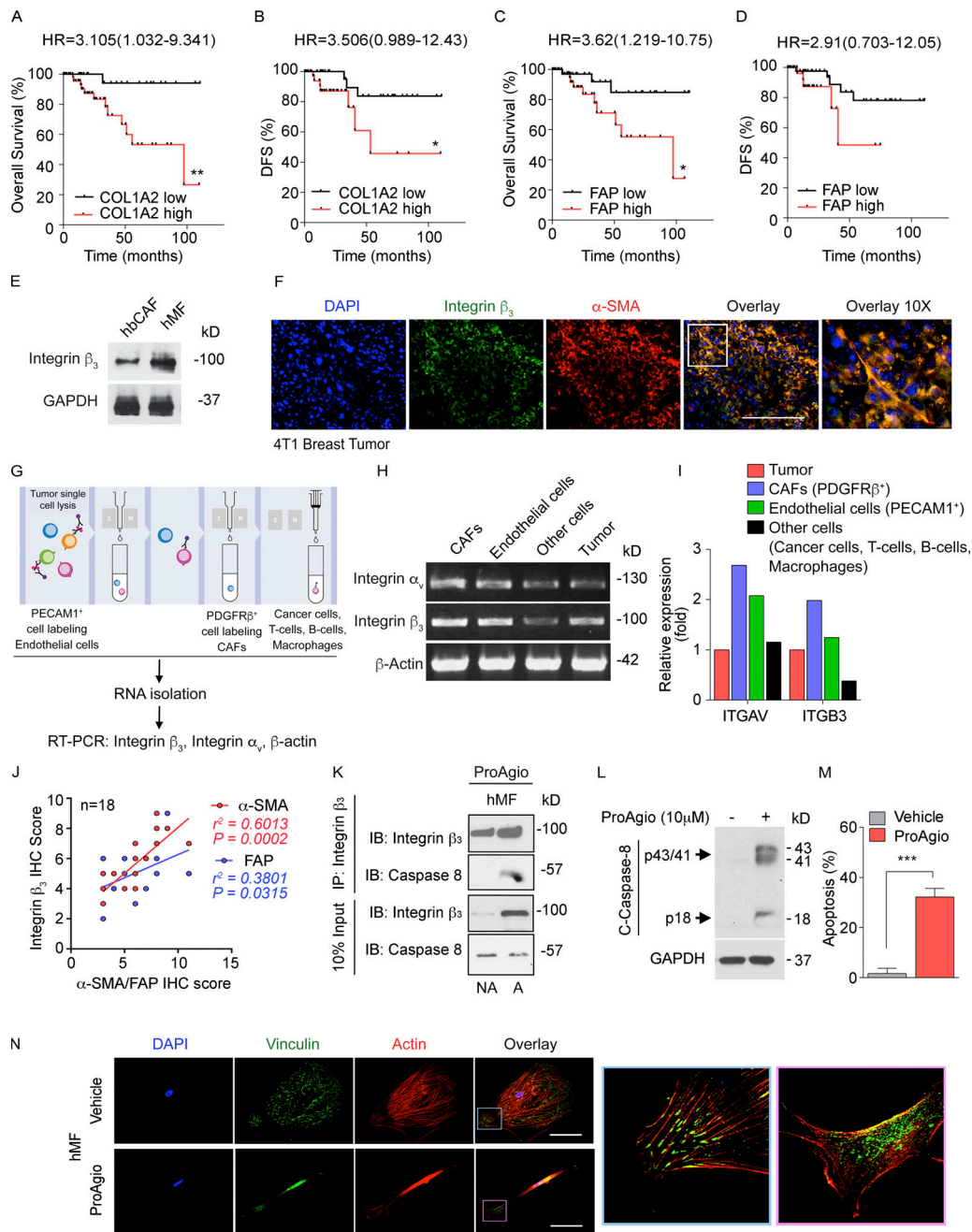
Figure S1. **High stroma is associated with poor overall survival and DFS; breast cancer CAFs express high levels of integrin $\alpha_v\beta_3$; there is a close correlation between integrin β_3, α-SMA, and FAP levels in TNBC patient tissue samples; and ProAgio induces apoptosis in breast cancer CAFs. (A–D)** Kaplan-Meier overall survival analyses of low and high COL1A2 (low, n = 34; high, n = 48; A) and FAP (low, n = 39; high, n = 43; C) and DFS of low and high COL1A2 (low, n = 40; high, n = 35; B) and FAP (low, n = 46; high, n = 29; D) gene expression in the tumors of TNBC patients. HR, hazard ratio. TCGA dataset of TNBC patients was obtained from cbioportal (https://www.cbioportal.org). **(E)** Level of integrin β_3 (IB: Integrin β_3) in hMFs and hbCAFs was analyzed by immunoblot. GAPDH is a loading control. **(F)** Representative images of IF costaining of α-SMA (red) and integrin β_3 (green) in the tumor sections of 4T1 mice. Nuclei were counterstained with DAPI (blue). Scale bar, 100 μm. **(G)** Schematic illustration of the MACS technique. **(H and I)** The mRNA levels (H) and quantification of integrin α_v (ITGAV) and integrin β_3 (ITGB3; I) in the indicated magnetically sorted cells from MMTV-PyMT breast tumor tissue were analyzed by RT-PCR (n = 2). β-actin is a loading control. **(J)** Correlation of integrin β_3 protein expression with α-SMA/FAP protein expression. Regression analysis for expression of the integrin β_3 (IHC) versus α-SMA/FAP (IHC) in tumor sections of TNBC patients (n = 18). **(K)** Co-immunoprecipitation (coIP) of caspase 8 with integrin β_3 (IP: Integrin β_3) was analyzed by immunoblot (IB: Caspase 8). Nonactivated hMFs (NA) and activeted hMFs (A) were treated with 5 μM ProAgio for 3 h. Immunoblot of integrin β_3 (IB: Integrin β_3) indicates the amount of β_3 that was coprecipitated down in the coIP. Input represents 10% of the total protein used for IP. **(L)** Levels of CC8 (IB: C-Caspase 8) in hbCAFs upon treatment with vehicle or 10 μM ProAgio for 3 h were analyzed by immunoblot. Immunoblot of GAPDH is a loading control. **(M)** Apoptosis in hbCAFs that were treated with 10 μM ProAgio (red bar) compared with vehicle (PBS, gray bar) was analyzed by apoptosis kit. **(N)** Representative images of Co-IF staining of vinculin (green) and rhodamine phalloidin (actin, red) of activated hMFs treated with vehicle or ProAgio. Nuclei were counterstained with DAPI (blue). Scale bars, 100 μm. All data are representative of at least three independent biological replicates. Error bars in M represent mean ± SEM. *, P < 0.05; **, P < 0.01; ***, P < 0.001 by log-rank test (A–D) or unpaired Student's t test (M).
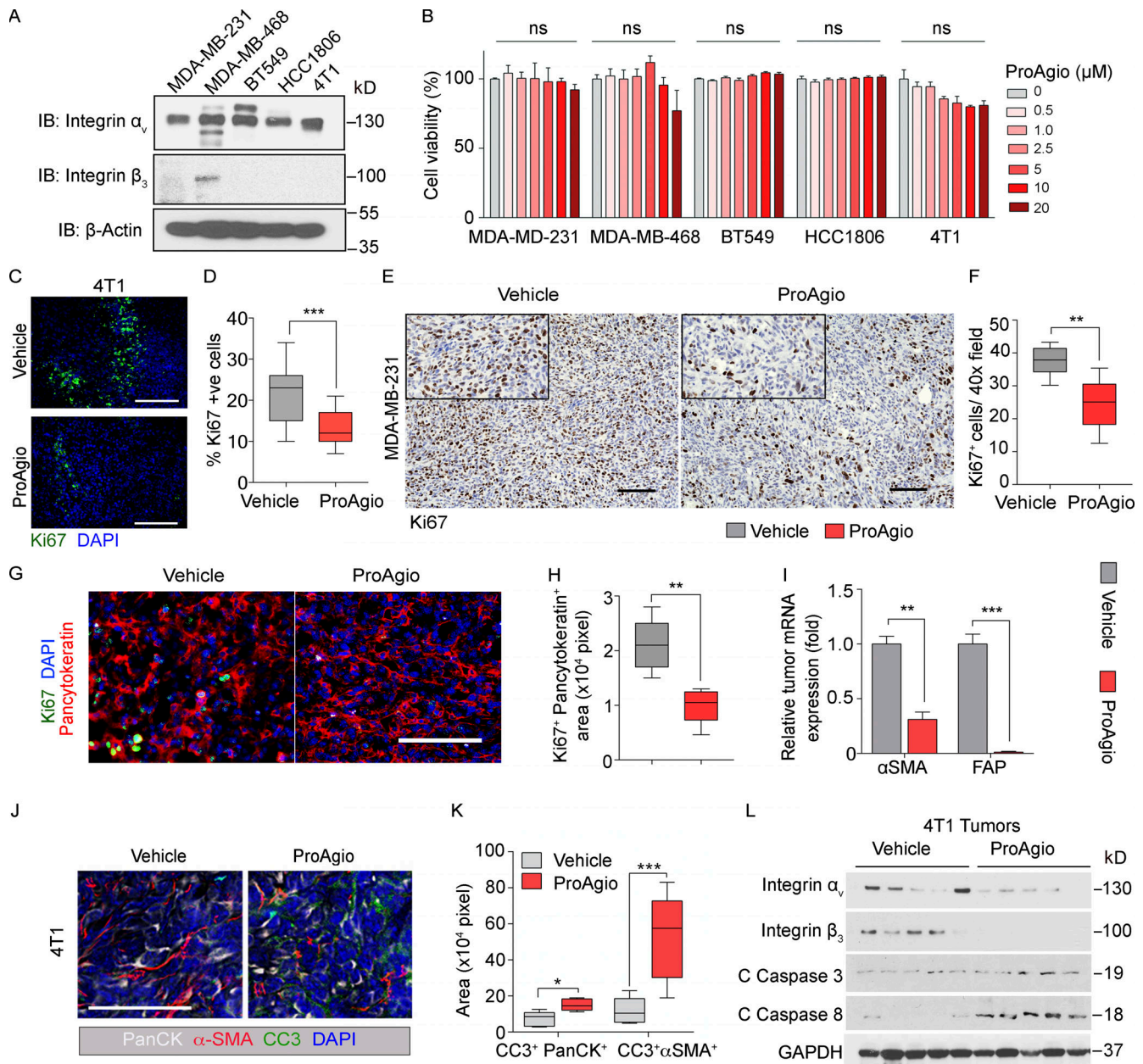
Figure S2. **ProAgio does not induce apoptosis in TNBC cell lines; ProAgio decreases cancer cell proliferation in mouse models; and ProAgio reduces levels of α-SMA by inducing apoptosis in breast cancer CAFs and mediates apoptosis in cancer cells. (A)** Levels of integrin α_V (IB: Integrin α_V) and integrin β_3 (IB: Integrin β_3) in the cell lysates of indicated TNBC cell lines were analyzed by immunoblot. β-actin is a loading control ($n = 2$). **(B)** Cell viability of indicated cells upon treatment with indicated concentrations of ProAgio for 24 h was analyzed by MTT assay. Experiments were performed at least in triplicate. **(C–F)** Representative images of IF staining (C, green) or IHC staining of Ki67 (E) and quantification of percentage of Ki67-positive cells in the sections of 4T1 tumor (D) or Ki67$^+$ area in the sections of MDA-MB-231 tumor (F) upon treatment with vehicle or ProAgio. Insets, ×1.5. $n = 6$–8/group. Scale bars, 100 μm. **(G and H)** Representative images of IF costaining of pancytokeratin (red) and Ki67 (green; G) and quantification of both Ki67$^+$pancytokeratin$^+$ area (H) in the tumor sections of 4T1 mice treated with vehicle or ProAgio. Nuclei were counterstained with DAPI (blue); $n = 5$/group. Scale bar, 100 μm. **(I)** mRNA levels of α-SMA (left panel) and FAP (right panel) measured by qRT-PCR in the tumors of 4T1 mice treated with vehicle (gray bar) or ProAgio (red bar; $n = 4$/group). **(J and K)** Representative images of three-color IF staining of pancytokeratin (PanCK, white), CC3 (green), and α-SMA (red; J) and quantification of CC3$^+$pancytokeratin$^+$ and CC3$^+$α-SMA$^+$ area (K) in tumor sections of 4T1 mice treated with vehicle or ProAgio. Nuclei were counterstained with DAPI (blue); $n = 5$–7/group. Scale bar, 50 μm. **(L)** Levels of integrin α_V (IB: Integrin α_V), integrin β_3 (IB: Integrin β_3), CC3 (IB: CC3), and CC8 (IB: C Caspase 8) in the 4T1 tumor tissue lysates of mice treated with vehicle or ProAgio were analyzed by immunoblot ($n = 5$). GAPDH is the loading control. Error bars in B and I represent mean ± SEM. *, $P < 0.05$; **, $P < 0.01$; ***, $P < 0.001$; ns denotes nonsignificant by unpaired Student's t test.
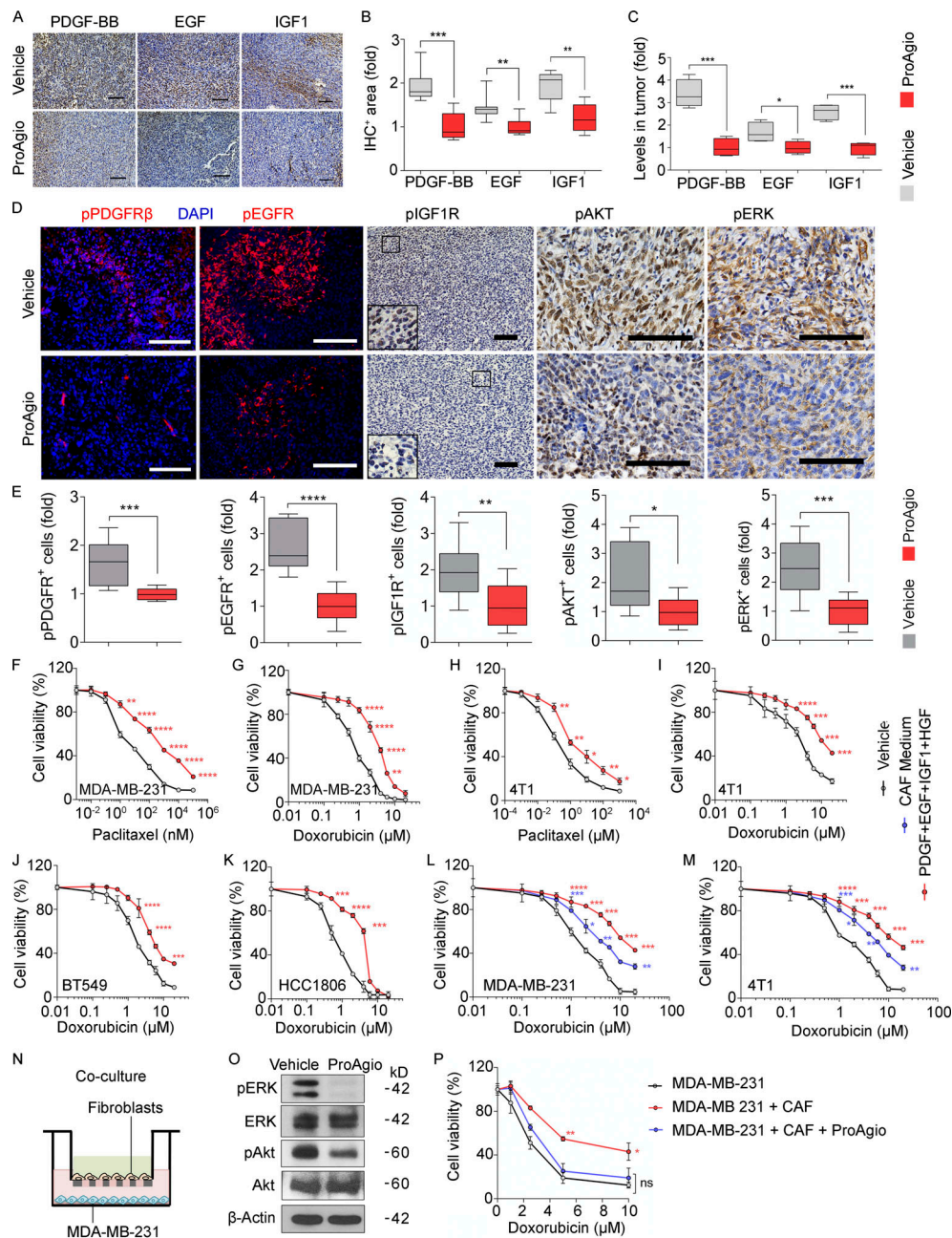
Figure S3. **ProAgio reduces levels of GFs and signaling downstream; the addition of GFs or CAF-conditioned media mediates apoptotic resistance in cancer cells; and ProAgio induces apoptosis in breast CAFs and therefore sensitizes cancer cells to apoptotic induction by a chemotherapeutic agent.** **(A and B)** Representative images of IHC staining of PDGF-BB, EGF, and IGF1 (A) and quantitative analysis of PDGF-BB, EGF, and IGF1-positive area (B) in the tumor sections of 4T1 mice treated with vehicle or ProAgio. Scale bars, 100 μm; n = 3–4/group. **(C)** Intratumoral levels of PDGF-BB, EGF, and IGF1 were determined by ELISA assay in the tumor extracts of 4T1 mice (n = 4/group). **(D and E)** Representative images of IF staining of pPDGFRβ, pEGFR, IHC staining of pIGF1R, pAKT, and pERK (D), and quantitative analysis of pPDGFRβ, pEGFR, pIGF1R, pAKT, and pERK-positive cells (E) in the tumor sections of 4T1 mice treated with vehicle or ProAgio. In IF images, nuclei were counterstained with DAPI (blue). The quantifications are presented as fold change using the ProAgio treatment group as a reference. Scale bars, 100 μm; n = 4–5/group. **(F–K)** Cell viability of TNBC cells, including MDA-MB-231 (F and G), 4T1 (H and I), BT549 (J), and HCC1806 (K) upon treatment with indicated concentrations of indicated drugs for 48 h in the culture media containing the vehicle (i.e., PBS [black line] or indicated GFs [red line]). **(L and M)** Cell viability of MDA-MB-231 (L) and 4T1 (M) cells upon treatment with indicated concentrations of DOX for 48 h in the culture media containing the conditioned medium from activated breast fibroblasts (blue line) or the indicated GFs (red line) compared with the vehicle (black line). **(N)** Schematic of the experimental setup for transwell for co-culture assay. **(O)** Levels of pERK and pAKT in MDA-MB-231 cells co-cultured with activated breast fibroblasts (CAFs) treated with vehicle or ProAgio were analyzed by immunoblot. β-actin is the loading control. **(P)** Cell viability of MDA-MB-231 cells upon treatment with indicated concentrations of DOX for 48 h in the activated human breast fibroblasts (CAFs) and MDA-MB-231 cells (red line) or the pretreated activated human breast fibroblasts (CAFs) and MDA-MB-231 cells with ProAgio (blue line) compared with vehicle (black line). ProAgio (5 μM) was added to the activated human breast fibroblasts (CAFs) for 6 h followed by DOX treatment for 48 h. Cell viability was analyzed by MTT assay. All data are representative of at least three independent biological replicates. Error bars represent mean ± SEM. *, P < 0.05; **, P < 0.01; ***, P < 0.001; ****, P < 0.0001; ns denotes nonsignificant by unpaired Student's t test.
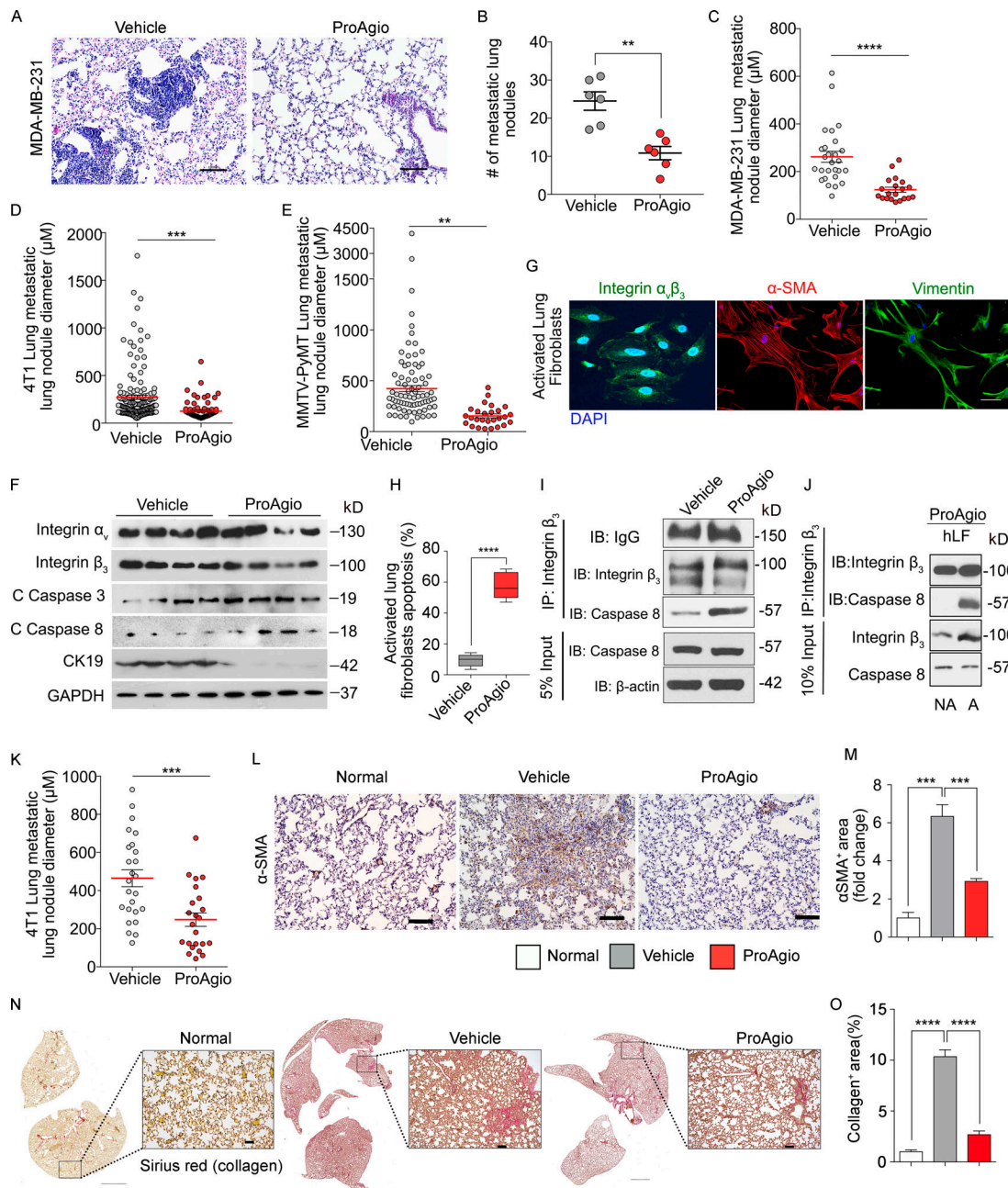
Figure S4. **ProAgio treatment reduces the number and size of metastatic lung nodules in mouse models, and ProAgio treatment induces apoptosis in integrin α$_v$β$_3$–expressing activated lung fibroblasts and decreases α-SMA and collagen levels in metastatic lungs in mouse models. (A–C)** Representative images of H&E staining of lungs (A) and quantification of metastatic lung nodule number (B) and lung metastatic nodule diameter (C) of MDA-MB-231 mice treated with vehicle or ProAgio (*n* = 6/group). **(D and E)** Quantification of the lung metastatic nodule diameter of 4T1 orthotopic (D) and MMTV-PyMT (E) mice treated with vehicle or ProAgio (*n* = 5 or 6/group). **(F)** Levels of integrin α$_V$ (IB: Integrin α$_V$), integrin β$_3$ (IB: Integrin β$_3$), CC3 (IB: C Caspase 3), CC8 (IB: C Caspase 8), and CK19 (IB: CK19) in the lung tissue lysates of 4T1 mice treated with vehicle or ProAgio were analyzed by immunoblot (*n* = 4). GAPDH is the loading control. **(G)** Representative images of IF staining of integrin α$_v$β$_3$ (green), α-SMA (red), and vimentin (green) in the activated hLFs. Nuclei were counterstained with DAPI (blue). Scale bar, 100 μm. **(H)** Apoptosis in activated lung fibroblasts that were treated with 5 μM ProAgio was analyzed by Annexin V kit. **(I)** Co-immunoprecipitation (coIP) of caspase 8 with integrin β$_3$ (IP: Integrin β$_3$) was analyzed by immunoblot. hLFs were activated with 5 ng/ml TGF-β for 48 h and subsequently treated with 5 μM ProAgio for 4 h before preparation of the extract. Immunoblot of integrin β$_3$ (IB: Integrin β$_3$) indicates the amount of integrin β$_3$ that was precipitated down in coIP. IgG is the loading control. Input represents 5% of the total protein used for IP, and β-actin is the loading control. **(J)** coIP of caspase 8 with integrin β$_3$ (IP: Integrin β$_3$) was analyzed by immunoblot (IB: Caspase 8). Nonactivated hLFs (NA) and activated hLFs (A) were treated with 5 μM ProAgio for 3 h. Immunoblot of integrin β$_3$ (IB: Integrin β$_3$) indicates the amount of β$_3$ that was coprecipitated down in the coIP. Input represents 10% of the total protein used for IP. Experiments were performed in triplicate. **(K)** Quantification of the lung metastatic nodule diameter from the lung sections of the 4T1 spontaneous mouse model (*n* = 5/group). **(L–O)** Representative images of IHC staining of α-SMA (L), Sirius red staining of collagen (N), and quantification of α-SMA–positive area (M) and collagen-positive area (O) in the lung sections of vehicle- or ProAgio-treated 4T1 spontaneous mice (tail vein model) compared with normal mice. Scale bars, 100 μm; scale bars in N, 1,000 μm (left panel); *n* = 5–6/group. Error bars represent mean ± SEM. **, P < 0.01; ***, P < 0.001; ****, P < 0.0001 by unpaired Student's *t* test.
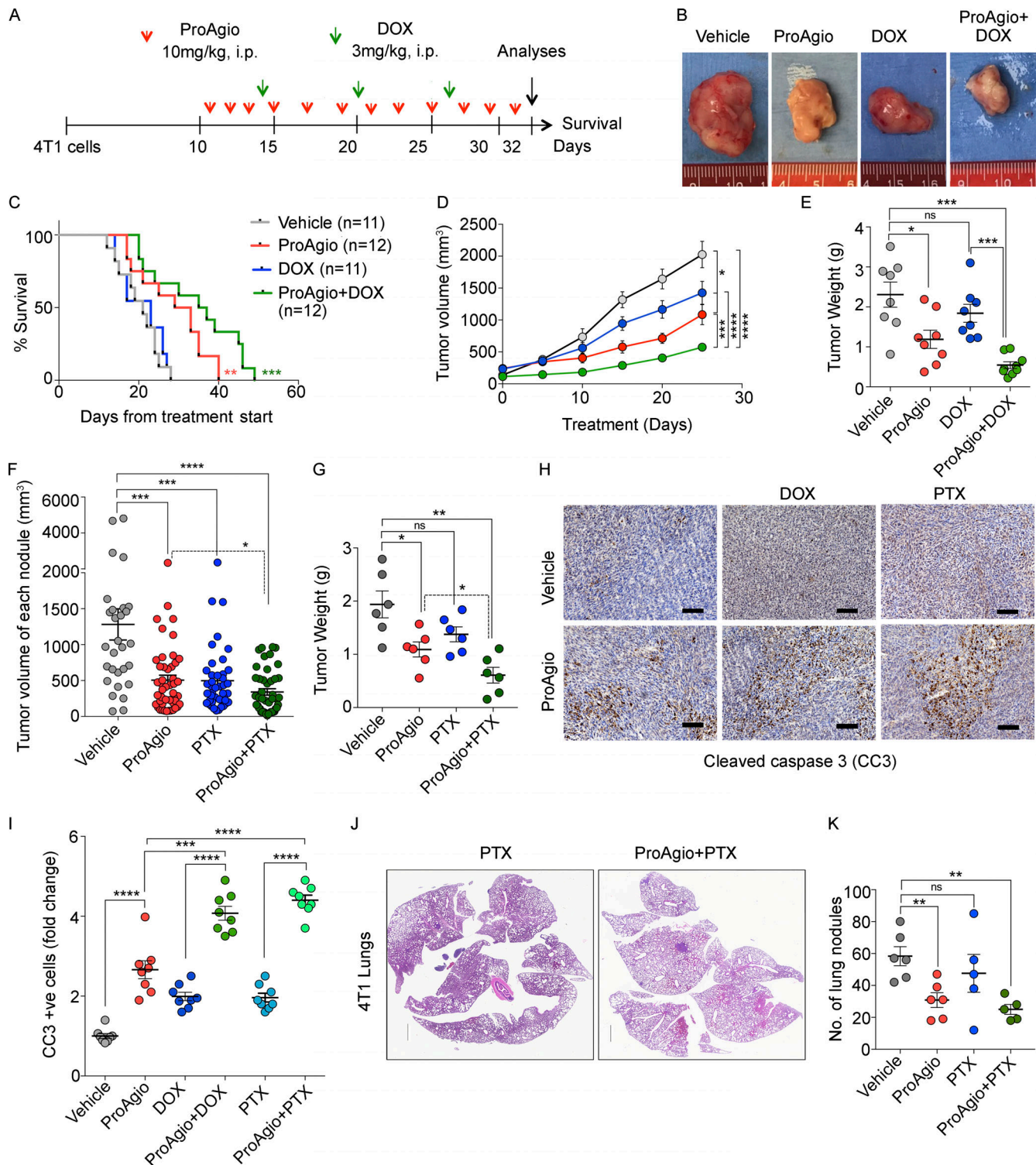
Figure S5. **ProAgio enhances the effect of chemotherapeutics in mouse models. (A)** Therapy regimen of 10 mg/kg ProAgio (i.p.) and 3 mg/kg DOX (i.p.) in 4T1 orthotopic mice. **(B)** Representative gross images of breast tumors of orthotopic 4T1 mice treated with indicated agents. **(C–E)** Kaplan-Meier survival analyses (n = 11–12; median survival [days]: vehicle = 21, ProAgio = 31, DOX = 23, ProAgio + DOX = 36; C), mean tumor volume (D), and mean tumor weight (E) of orthotopic 4T1 mice treated with indicated agents. **(F and G)** Mean tumor volume of each nodule (F) and average tumor weight (G) of MMTV-PyMT mice treated with indicated agents (n = 6–8). **(H and I)** Representative IHC images of CC3 staining (H) and quantification of CC3-positive cells (I) in 4T1 mice treated with indicated agents. Scale bars, 100 µm; n = 8/group. **(J and K)** Representative H&E staining of lungs (J), and quantification of lung nodules number (K) in 4T1 mice upon treatment with indicated agents; n = 5 or 6/group. Scale bars, 1,000 µm. Error bars represent mean ± SEM. *, $P < 0.05$; **, $P < 0.01$; ***, $P < 0.001$; ****, $P < 0.0001$; ns denotes nonsignificant by unpaired Student's t test.

Provided online is Table S1, which shows cell lines, reagents, antibodies, PCR primers, and kits used in this study.